

Insensitivity of Magnetic Coupling to Ligand Substitution in a Series of Tetraoxolene Radical-Bridged Fe₂ Complexes

Agnes E. Thorarinsdottir, Ragnar Bjornsson, and T. David Harris*



Cite This: <https://dx.doi.org/10.1021/acs.inorgchem.9b03736>



Read Online

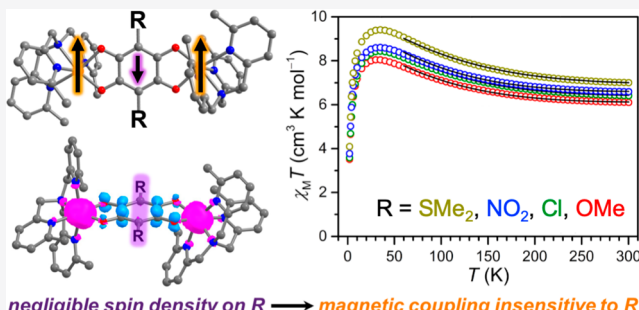
ACCESS |

Metrics & More

Article Recommendations

Supporting Information

ABSTRACT: The elucidation of magnetostructural correlations between bridging ligand substitution and strength of magnetic coupling is essential to the development of high-temperature molecule-based magnetic materials. Toward this end, we report the series of tetraoxolene-bridged Fe^{II}₂ complexes [(Me₃TPyA)₂Fe₂(^RL)]ⁿ⁺ (Me₃TPyA = tris(6-methyl-2-pyridylmethyl)amine; n = 2: O^{Me}LH₂ = 3,6-dimethoxy-2,5-dihydroxy-1,4-benzoquinone, ClLH₂ = 3,6-dichloro-2,5-dihydroxy-1,4-benzoquinone, Na₂[^{NO₂}L] = sodium 3,6-dinitro-2,5-dihydroxy-1,4-benzoquinone; n = 4: S^{Me}L = 3,6-bis(dimethylsulfonium)-2,5-dihydroxy-1,4-benzoquinone diylide) and their one-electron-reduced analogues. Variable-temperature dc magnetic susceptibility data reveal the presence of weak ferromagnetic superexchange between Fe^{II} centers in the oxidized species, with exchange constants of J = +1.2(2) (R = OMe, Cl) and +0.3(1) (R = NO₂, SMe₂) cm⁻¹. In contrast, X-ray diffraction, cyclic voltammetry, and Mössbauer spectroscopy establish a ligand-centered radical in the reduced complexes. Magnetic measurements for the radical-bridged species reveal the presence of strong antiferromagnetic metal–radical coupling, with J = -57(10), -60(7), -58(6), and -65(8) cm⁻¹ for R = OMe, Cl, NO₂, and SMe₂, respectively. The minimal effects of substituents in the 3- and 6-positions of ^RL^{x-}• on the magnetic coupling strength is understood through electronic structure calculations, which show negligible spin density on the substituents and associated C atoms of the ring. Finally, the radical-bridged complexes are single-molecule magnets, with relaxation barriers of U_{eff} = 50(1), 41(1), 38(1), and 33(1) cm⁻¹ for R = OMe, Cl, NO₂, and SMe₂, respectively. Taken together, these results provide the first examination of how bridging ligand substitution influences magnetic coupling in semiquinoid-bridged compounds, and they establish design criteria for the synthesis of semiquinoid-based molecules and materials.



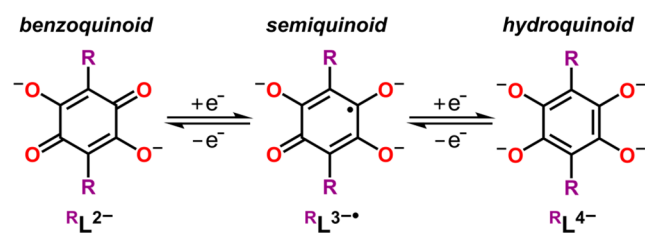
INTRODUCTION

Molecule-based magnetic materials, ranging from discrete mono- and multinuclear metal complexes¹ to extended networks,^{2–9} have garnered tremendous interest over the past few decades owing predominately to their potential advantages over established solid-state inorganic materials, such as adjustable chemical compositions, access through low-temperature synthetic routes, and chemical processability.^{4d,6g,8–10} Moreover, the employment of bridging ligands with predictable binding modes, such as cyanide and a wide range of organic linkers, grants exquisite synthetic control over both the bulk crystal structure and the local metal coordination environment and, therefore, enables the directed assembly of compounds with targeted structures and properties.^{5,6,8,11–15} Indeed, molecule-based materials may provide a new generation of designer magnets, with the potential to transform our current energy landscape through their utilization in technologies such as spin-based data processing, magnetoresistive sensing, magnetic gas separations, and permanent magnet generators.^{8,16–18} Nevertheless, for many of these applications to be realized, the operating temperatures of

molecule-based magnets must be increased to near or even above room temperature.

In targeting molecule-based magnets with high operating temperatures, the strength of magnetic exchange interactions between spin centers, quantified by the exchange constant J, represents a vitally important parameter. Specifically, the value of J between paramagnetic centers is directly correlated to the isolation of the spin ground state of single-molecule magnets,¹⁹ the relaxation barrier of single-chain magnets,²⁰ and the magnetic ordering temperature of permanent magnets.²¹ Despite this critical relationship between operating temperature and J, the vast majority of molecule-based magnets feature paramagnetic metal centers that are coupled through diamagnetic bridging ligands via a superexchange mechanism.

Received: December 24, 2019

Scheme 1. Redox Series^a

^aRedox series of deprotonated tetraoxolenes, which can act as bis(bidentate) bridging ligands.

While superexchange interactions through short oxo and cyano ligands can be sufficiently strong to, for instance, afford magnets that order above room temperature,^{5c,d,6b,11b} the magnitude of J decreases dramatically as the number of atoms in the bridging ligand increases,^{8b,c} thereby hindering the development of materials based on strong superexchange coupling through chemically tunable organic bridging ligands.

As an alternative to superexchange coupling, one key strategy to promote strong magnetic coupling involves the incorporation of a radical bridging ligand between paramagnetic metal ions, so as to engender strong direct magnetic exchange by virtue of direct overlap of the metal- and radical-based molecular orbitals.^{1u,13,22} Indeed, this approach has found significant success, as exemplified by extensive studies on systems featuring nitroxide,^{1u,2a,e,p,23} organonitrile,^{4,14a–c,24} perchlorotriphenylmethyl,²⁵ triplet carbene,²⁶ and pyrazine²⁷ radical ligands. Nevertheless, the low charges and monodentate binding mode of the coordinating functional groups in these ligands often limit the strength of metal–ligand interactions and hamper the directed assembly of compounds with well-defined structures.

Bis(bidentate) benzoquinoid ligands offer an appealing platform for the construction of radical-bridged compounds with strong magnetic coupling, as these ligands (i) undergo facile redox chemistry to generate the semiquinoid radical (see Scheme 1), (ii) form strong metal–ligand bonds and compounds with predictable structures owing to their bis(bidentate) binding mode and large negative charge, and (iii) display a high capacity for chemical modification, where a wide range of donor atoms and ring-bound substituents can be readily installed. Indeed, a number of dinuclear complexes,^{1b,28,29} chain compounds,^{2w,30} and extended networks^{9,31} featuring semiquinoid bridging ligands have already been shown to exhibit strong metal–radical interactions. Nevertheless, despite the tremendous potential of quinoid-

based ligands in the development of magnetic materials, systematic studies that probe the effects of ligand substitution on the magnetic coupling strength in semiquinoid-bridged systems are conspicuously lacking. The elucidation of these magnetostructural correlations is essential to derive a clear and complete understanding of the factors that govern the strength and sign of magnetic coupling in metal-semiquinoid compounds, and such efforts may ultimately inform the design of molecule-based magnets with high operating temperatures.

The strength of magnetic exchange through diamagnetic benzoquinoid ligands has previously been found to vary with the electronic properties of the ring-bound substituents in Cu^{II}_2 complexes³² and two-dimensional (2D) ferrimagnets.^{14g,33} While the substituent effects are substantial for 2D $\text{Mn}^{\text{II}}\text{Cr}^{\text{III}}$ frameworks, leading to a twofold increase in magnetic ordering temperature when the electronegativity of the substituents is decreased,³³ these effects are subtle for Cu^{II}_2 complexes due to a weak contribution from the substituents to the magnetic orbitals.³² Furthermore, remote ligand substitution can vary the coupling strength by nearly threefold in mononuclear Mn^{II} and Cu^{II} semiquinoid complexes.³⁴ Here, electron-withdrawing substituents were found to provide stronger ferromagnetic interactions than electron-donating substituents for the Cu^{II} complexes. In contrast, no clear trend was observed for the antiferromagnetically coupled Mn^{II} analogues, which was postulated to stem from the presence of multiple convoluting exchange pathways.³⁴ These studies notwithstanding, a systematic investigation of the electronic effects of ligand substituents on magnetic coupling in semiquinoid-bridged compounds remains elusive.

Herein, we report the series of tetraoxole-bridged Fe^{II}_2 complexes $[(\text{Me}_3\text{TPyA})_2\text{Fe}_2(^{\text{R}}\text{L}^{x-})]^{n+}$ ($x = 2, n = 2$: R = OMe, Cl, NO_2 ; $x = 0, n = 4$: R = SMe₂; Me₃TPyA = tris(6-methyl-2-pyridylmethyl)amine) and the radical-bridged congeners $[(\text{Me}_3\text{TPyA})_2\text{Fe}_2(^{\text{R}}\text{L}^{x-}\bullet)]^{n+}$ ($x = 3, n = 1$: R = OMe, Cl, NO_2 ; $x = 1, n = 3$: R = SMe₂). While the identity of R is shown to substantially influence the strength of superexchange interactions through the diamagnetic tetraoxole, it has remarkably little impact on the strength of the metal–radical interaction in the radical-bridged analogues despite the presence of substituents with immensely different electronic character across the series. To our knowledge, this study provides the first systematic examination of how ligand substitution influences J in semiquinoid-bridged compounds, and it establishes synthetic design criteria to be considered in the construction of future semiquinoid-based materials.

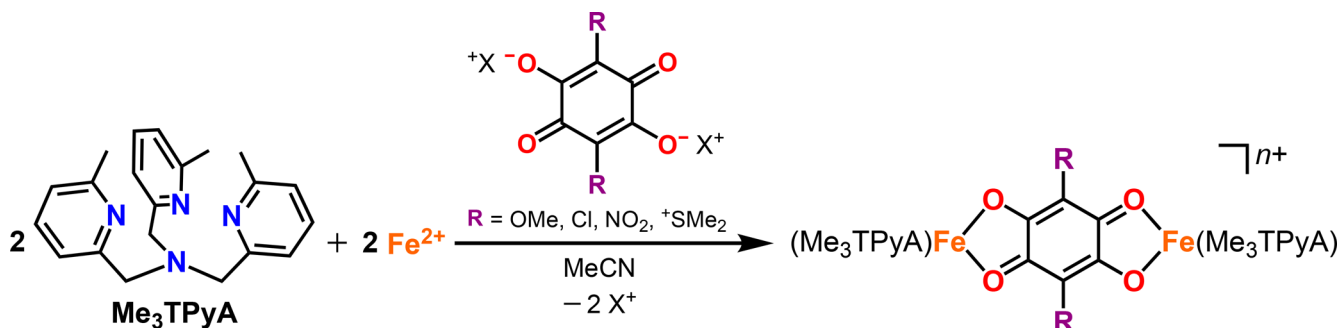


Figure 1. Synthesis of complexes $[(\text{Me}_3\text{TPyA})_2\text{Fe}_2(^{\text{R}}\text{L}^{x-})]^{n+}$ (R = OMe, Cl, NO_2 , SMe₂), as observed in **1-OMe** ($n = 2$), **1-Cl** ($n = 2$), **1-NO₂** ($n = 2$), and **1-SMe₂** ($n = 4$). X = H for R = OMe, Cl; X = Na for R = NO_2 ; X = nothing for R = SMe₂.

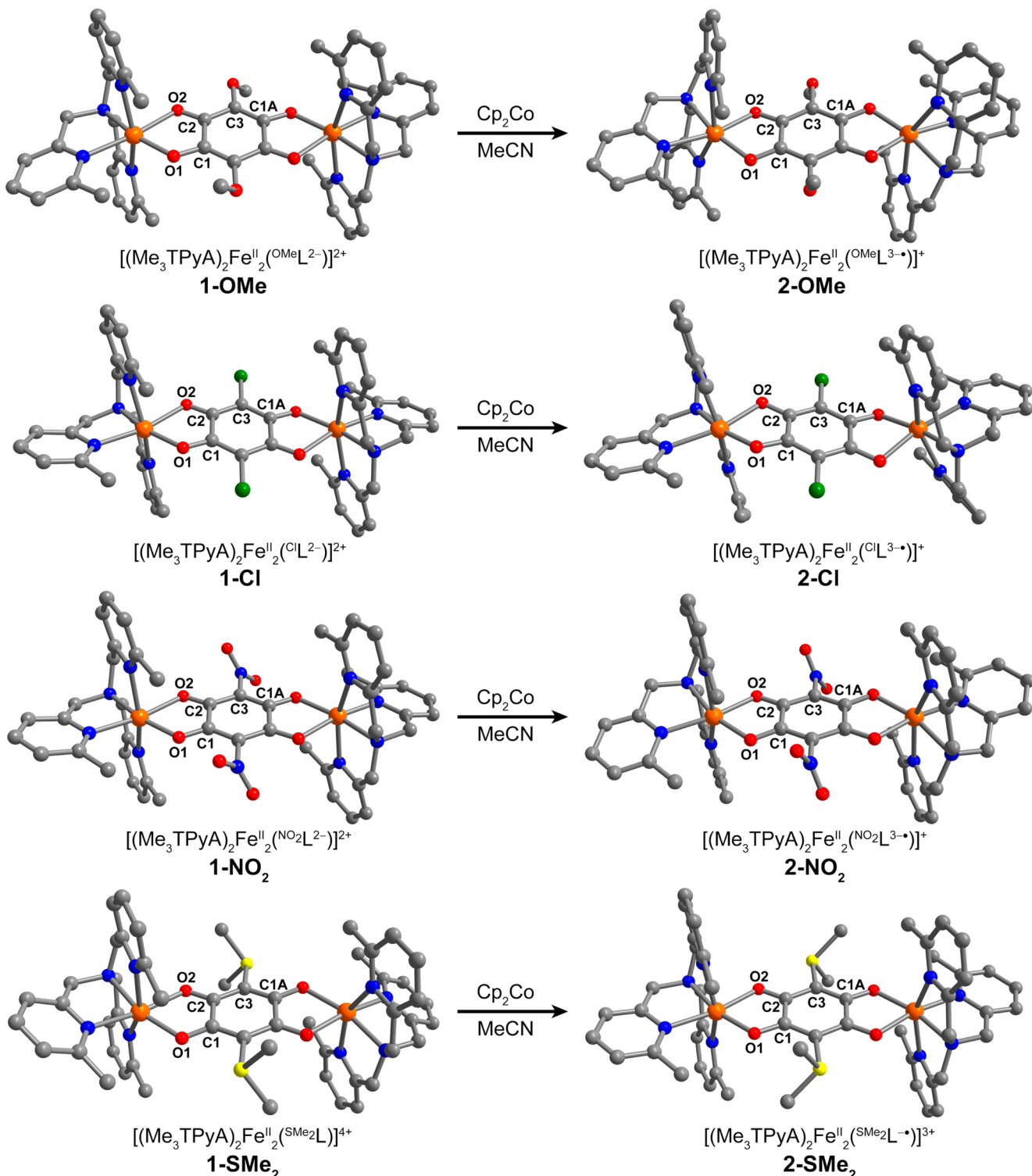


Figure 2. Crystal structures of the cationic complexes $[(\text{Me}_3\text{TPyA})_2\text{Fe}_2(\text{R}^{\text{L}})]^{4+/2+}$ (left) and $[(\text{Me}_3\text{TPyA})_2\text{Fe}_2(\text{R}^{\text{L}})]^{3+/1+}$ (right), as observed in **1**-R-solvent and **2**-R-solvent (R = OMe, Cl, NO₂, SMe₂), respectively. Orange, green, yellow, red, blue, and gray spheres represent Fe, Cl, S, O, N, and C atoms, respectively; H atoms are omitted for clarity.

RESULTS AND DISCUSSION

Syntheses, Structures, and Electrochemistry. With the aim to better understand the effects of ligand substitution on electron delocalization and magnetic coupling in semiquinoid radical-bridged magnets, we employed dinuclear complexes as model systems owing to their structural simplicity and ease of magnetic characterization. Specifically, we targeted a series of

isostructural Fe^{II}_2 complexes bridged by tetraoxolene derivatives with an array of substituents in the 3- and 6-positions, ranging from electron-donating OMe groups to strongly electron-withdrawing ⁴SMe₂ groups.

Reaction of ⁴R¹H₂ (R = OMe, Cl), Na₂[⁴NO₂L], or ⁴SMe₂L·2CH₃COOH with 2 equiv each of $\text{Fe}(\text{BF}_4)_2 \cdot 6\text{H}_2\text{O}$ and Me₃TPyA in MeCN, followed by purification and subsequent

Table 1. Selected Mean Interatomic Distances (\AA) and Octahedral Distortion Parameter (\sum_{sum}) for the Cationic Complexes in 1-R-Solvent and 2-R-Solvent^{a,b}

	1-OMe· 4.0MeCN	2-OMe· 2.0MeCN	1-Cl· 0.7H ₂ O	2-Cl· 0.5Et ₂ O	1-NO ₂ · 4.0MeCN	2-NO ₂	1-SMe ₂ · 4.0MeCN	2-SMe ₂ ·0.9MeCN· 0.5Et ₂ O
Fe—N	2.210(2)	2.2466(6)	2.195(3)	2.234(2)	2.1998(5)	2.2223(7)	2.196(2)	2.227(1)
Fe—O1	2.003(3)	1.992(1)	2.051(5)	1.991(3)	2.0372(8)	2.010(2)	2.039(2)	2.038(2)
Fe—O2	2.203(3)	2.112(1)	2.187(3)	2.130(3)	2.1782(9)	2.143(1)	2.210(3)	2.140(2)
Fe—O	2.103(3)	2.052(1)	2.119(3)	2.060(2)	2.1077(6)	2.076(1)	2.125(2)	2.084(1)
C1—O1	1.294(5)	1.313(2)	1.269(6)	1.304(5)	1.258(2)	1.293(2)	1.254(4)	1.292(3)
C2—O2	1.245(5)	1.294(2)	1.238(8)	1.283(5)	1.240(2)	1.278(2)	1.240(3)	1.280(3)
C—O	1.270(4)	1.304(2)	1.254(5)	1.293(4)	1.249(1)	1.285(2)	1.247(3)	1.286(2)
C1—C2	1.516(6)	1.470(2)	1.532(9)	1.468(5)	1.532(2)	1.465(2)	1.526(4)	1.465(3)
C2—C3	1.429(6)	1.407(2)	1.409(7)	1.403(5)	1.411(2)	1.404(2)	1.404(4)	1.416(3)
C3—C1A	1.363(6)	1.389(2)	1.389(9)	1.395(6)	1.386(2)	1.396(2)	1.388(4)	1.408(3)
C—C	1.436(4)	1.422(1)	1.443(5)	1.422(3)	1.443(1)	1.422(2)	1.439(3)	1.430(2)
Fe···Fe ^c	7.996(3)	7.8652(9)	8.018(2)	7.823(2)	8.0219(8)	7.9330(9)	8.017(3)	7.9972(6)
\sum_{sum}^d	106.3(5)	125.8(2)	110.2(7)	112.3(4)	109.8(2)	111.7(2)	111.2(3)	110.1(3)

^aSee Figure 2 for the atomic numbering scheme. ^bAverage distances for specific types of bonds are shown in bold. ^cIntramolecular Fe···Fe distance.

^dOctahedral distortion parameter (\sum_{sum}) = sum of the absolute deviation from 90° for the 12 *cis* angles in [FeN₄O₂].³⁹

crystallization, afforded the compounds [(Me₃TPyA)₂Fe₂(^{OMe}L)](BF₄)₂ (**1-OMe**), [(Me₃TPyA)₂Fe₂(^{Cl}L)](BF₄)₂·0.3H₂O (**1-Cl**), [(Me₃TPyA)₂Fe₂(^{NO₂}L)](BF₄)₂ (**1-NO₂**), and [(Me₃TPyA)₂Fe₂(^{SMe₂}L)](BF₄)₄ (**1-SMe₂**) as dark green crystalline solids (see Figure 1). Slow diffusion of Et₂O vapor into concentrated MeCN solutions of **1-R** (R = OMe, Cl, NO₂, SMe₂) gave dark orange plate-shaped crystals of **1-OMe**·4.0MeCN, **1-Cl**·0.7H₂O, **1-NO₂**·4.0MeCN, and **1-SMe₂**·4.0MeCN suitable for single-crystal X-ray diffraction analysis. All compounds crystallized in the triclinic space group *P*̄*I*, with the exception of **1-SMe₂**·4.0MeCN, which crystallized in the monoclinic space group *P*2₁/c (see Tables S1–S4). In general, the structures of [(Me₃TPyA)₂Fe₂(^RL)]ⁿ⁺ (*n* = 2: R = OMe, Cl, NO₂; *n* = 4: R = SMe₂) consist of two crystallographically equivalent [(Me₃TPyA)Fe]²⁺ moieties connected by a deprotonated ^RL^{x-} (*x* = 2: R = OMe, Cl, NO₂; *x* = 0: R = SMe₂) bridging ligand, with a crystallographic site of inversion located at the center of ^RL^{x-} (see Figure 2). Each Fe^{II} center resides in a distorted octahedral coordination environment comprised of two *cis*-oriented O atoms from ^RL^{x-} (*x* = 2: R = OMe, Cl, NO₂; *x* = 0: R = SMe₂) and four N atoms from the Me₃TPyA capping ligand.

The mean Fe—N and Fe—O bond distances across the series fall in the ranges of 2.195(3)–2.210(2) Å and 2.103(3)–2.125(2) Å, respectively, consistent with reported distances for high-spin *S* = 2 Fe^{II} centers in similar coordination environments (see Table 1).^{28d,35–37} Within the bridging ligand, the average C—O distance ranges from 1.247(3) to 1.270(4) Å across the series, which falls between the value expected for a single and a double bond.³⁸ Moreover, the mean C1—C2 bond distance of 1.516(6)–1.532(9) Å, typical for a single bond, is substantially longer than the average C2—C3 and C3—C1A bond distances, which range from 1.404(4) to 1.429(6) Å and from 1.363(6) to 1.389(9) Å, respectively, across the series. These collective distances strongly suggest that the bridging ligand in **1-OMe**·4.0MeCN, **1-Cl**·0.7H₂O, **1-NO₂**·4.0MeCN, and **1-SMe₂**·4.0MeCN is best described as two localized 6-π-electron fragments connected by two C—C single bonds. The observation of two drastically different Fe—O bond distances, specifically shorter Fe—O1 distances of 2.003(3)–2.051(5) Å and longer Fe—O2 distances of 2.1782(9)–2.210(3) Å, further supports the formulation of the bridging ligand in these

compounds as the diamagnetic ^RL^{x-} (*x* = 2: R = OMe, Cl, NO₂; *x* = 0: R = SMe₂). Finally, the Fe^{II}₂ complexes in **1-OMe**·4.0MeCN, **1-Cl**·0.7H₂O, **1-NO₂**·4.0MeCN, and **1-SMe₂**·4.0MeCN feature a mean intramolecular Fe···Fe distance ranging from 7.996(3) to 8.0219(8) Å, in accord with values reported for other high-spin benzoquinoid-bridged Fe^{II}₂ compounds.^{28d,29a,36} Notably, the similar structural metrics for **1-OMe**·4.0MeCN, **1-Cl**·0.7H₂O, **1-NO₂**·4.0MeCN, and **1-SMe₂**·4.0MeCN indicate that the solid-state structure of this family of Fe^{II}₂ complexes is minimally affected by the nature of the benzoquinoid substituents. Furthermore, comparison of the average Fe—O distances and the octahedral distortion parameters (\sum_{sum})³⁹ in **1-R**-solvent to values reported for analogous tetraoxolene-bridged Fe^{II}₂ complexes bearing TPyA capping ligands (Fe—O = 2.089(2)–2.138(2) Å; $\sum_{\text{sum}} = 121.6(5)$ –185.4(3)°)^{28,37} illustrates the lack of significant steric effects imposed by the Me groups of Me₃TPyA on the Fe^{II} coordination environment in **1-R**-solvent.

To probe the effects of tetraoxolene substitution on the electronic structure of **1-R** and to assess the feasibility of isolating the radical-bridged congeners, cyclic voltammetry experiments were performed for MeCN solutions of these compounds at 298 K. The cyclic voltammograms of **1-R** are depicted in Figure 3. Each voltammogram exhibits two reversible processes at $E_{1/2} = +0.22$ and -1.11 V, $+0.33$ and -0.86 V, $+0.41$ and -0.58 V, and $+0.45$ and -0.47 V versus [Cp₂Fe]^{0/1+} for **1-OMe**, **1-Cl**, **1-NO₂**, and **1-SMe₂**, respectively. On the basis of precedent in other benzoquinoid-bridged Fe₂ complexes, we assign the wave at negative potential to the ligand-centered redox process ^RL^{x-(x+1)-•} (*x* = 2: R = OMe, Cl, NO₂; *x* = 0: R = SMe₂) and the wave at positive potential to the metal-based Fe^{II}Fe^{II}/Fe^{II}Fe^{III} couple.^{28d,29a,b,40} The variation of $E_{1/2}$ with the identity of the substituents for both ligand- and metal-based processes correlates linearly with the Hammett substituent constant (σ_p), which quantifies the electronic properties of substituents by considering both inductive and resonance effects (see Figures S1 and S2).⁴¹ In particular, $E_{1/2}$ for the Fe^{II}Fe^{II}/Fe^{II}Fe^{III} couple is anodically shifted by 0.23 V as the substituents are varied from electron-donating OMe groups to strongly electron-withdrawing ⁺SMe₂ groups, while the concurrent anodic shift in $E_{1/2}$ for the ligand-centered process is 0.64 V. The more

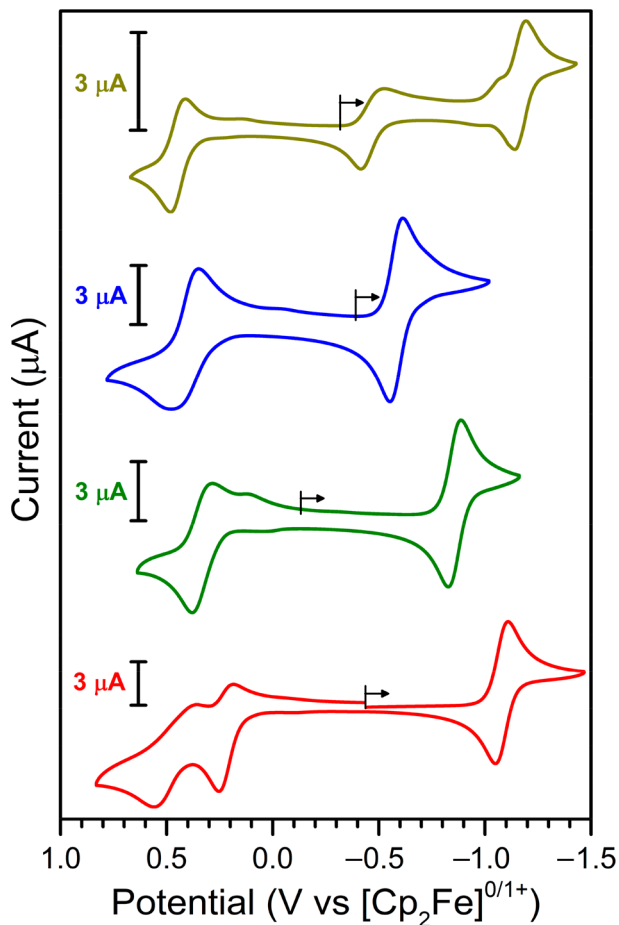


Figure 3. Cyclic voltammograms for solutions of **1-R** in MeCN containing 100 mM $(\text{Bu}_4\text{N})\text{(PF}_6)$ supporting electrolyte, collected at 298 K; R = OMe (red), Cl (green), NO_2 (blue), SMe_2 (gold). Scan rate = 100 mV s^{-1} for R = OMe, Cl, NO_2 ; 25 mV s^{-1} for R = SMe_2 . Black vertical lines and arrows denote the open-circuit potentials and scan directions, respectively.

pronounced change in $E_{1/2}$ for ${}^{\text{R}}\text{L}^{x-/(x+1)-\bullet}$ ($x = 2$: R = OMe, Cl, NO_2 ; $x = 0$: R = SMe_2) is consistent with the substituents primarily affecting the energy levels of the ligand; however, the clear variation in the metal-based redox potential indicates that the electronic properties of the substituents significantly modulate the metal–ligand interactions as well. The remaining oxidation event at +0.56 V versus $[\text{Cp}_2\text{Fe}]^{0/1+}$ for **1-OMe** is assigned to the metal-based $\text{Fe}^{\text{II}}\text{Fe}^{\text{III}}/\text{Fe}^{\text{III}}\text{Fe}^{\text{III}}$ oxidation, whereas the additional reversible redox event at $E_{1/2} = -1.17$ V versus $[\text{Cp}_2\text{Fe}]^{0/1+}$ for **1-SMe₂** is assigned to the ligand-based ${}^{\text{SMe}_2}\text{L}^{-\bullet/2-}$ couple.

Together, the cyclic voltammetry measurements suggest that the radical-bridged Fe^{I}_2 complexes $[({\text{Me}_3\text{TPyA}})_2\text{Fe}_2({}^{\text{R}}\text{L}^{x-\bullet})]^{n+}$ ($x = 3, n = 1$: R = OMe, Cl, NO_2 ; $x = 1, n = 3$: R = SMe_2) should be chemically accessible. Toward this end, dark green MeCN solutions of **1-R** were treated with stoichiometric quantities of the reductant Cp_2Co to give red-brown (R = OMe, Cl, NO_2) or green-brown (R = SMe_2) solutions. ^1H NMR analysis revealed the formation of new paramagnetic species (see Figures S3–S16) with generally more broad peaks relative to the oxidized analogues. Subsequent diffusion of Et_2O vapor into these solutions afforded red-orange (R = OMe, Cl, NO_2) or orange (R = SMe_2) plate-shaped crystals of the one-electron reduced

compounds $[({\text{Me}_3\text{TPyA}})_2\text{Fe}_2({}^{\text{OMe}}\text{L})](\text{BF}_4)\cdot 2.0\text{MeCN}$ (**2-OMe**·2.0MeCN), $[({\text{Me}_3\text{TPyA}})_2\text{Fe}_2({}^{\text{Cl}}\text{L})](\text{BF}_4)\cdot 0.5\text{Et}_2\text{O}$ (**2-Cl**·0.5Et₂O), $[({\text{Me}_3\text{TPyA}})_2\text{Fe}_2({}^{\text{NO}_2}\text{L})](\text{BF}_4)$ (**2-NO₂**), and $[({\text{Me}_3\text{TPyA}})_2\text{Fe}_2({}^{\text{SMe}_2}\text{L})](\text{BF}_4)_3\cdot 0.9\text{MeCN}\cdot 0.5\text{Et}_2\text{O}$ (**2-SMe₂**·0.9MeCN·0.5Et₂O). Subsequent drying of these crystals under reduced pressure gave the desolvated forms **2-R** (R = OMe, Cl, NO_2 , SMe_2) in moderate yields of 57–88%. IR spectroscopy for solid samples reveals changes in peak frequencies and intensities in the 1200–1600 cm^{-1} spectral range when moving from **1-R** to **2-R** (R = OMe, Cl, NO_2 , SMe_2) (see Figures S17–S22), suggesting different net C–C and/or C–O bond order for the tetraoxolene bridging ligand in these two series of compounds.

The cationic complexes $[({\text{Me}_3\text{TPyA}})_2\text{Fe}_2({}^{\text{OMe}}\text{L})]^+$, $[({\text{Me}_3\text{TPyA}})_2\text{Fe}_2({}^{\text{Cl}}\text{L})]^+$, $[({\text{Me}_3\text{TPyA}})_2\text{Fe}_2({}^{\text{NO}_2}\text{L})]^+$, and $[({\text{Me}_3\text{TPyA}})_2\text{Fe}_2({}^{\text{SMe}_2}\text{L})]^{3+}$ in **2-R**-solvent feature very similar structures to those in **1-R**-solvent. The two Fe^{II} sites in each molecule are related through a crystallographic inversion center, with the exception of slightly inequivalent Fe^{II} centers in $[({\text{Me}_3\text{TPyA}})_2\text{Fe}_2({}^{\text{Cl}}\text{L})]^+$ stemming from crystal packing of the $(\text{BF}_4)^-$ counterion. The nearly identical values of \sum_{sum}^{39} for **1-R**-solvent and **2-R**-solvent illustrate that the coordination geometry at Fe^{II} is not significantly affected by the substituents and redox state of the bridging ligand. In contrast, close comparison of the bond distances between the two series of compounds reveals several key differences. First, the mean C–C bond distance decreases slightly by 0.6–1.5%, from 1.436(4)–1.443(5) to 1.422(1)–1.430(2) Å, in moving from **1-R**-solvent to **2-R**-solvent. Moreover, the mean C–O bond distance for **2-R**-solvent varies from 1.285(2) to 1.304(2) Å across the series, which represents a 2.7–3.1% increase as compared to the values obtained for the oxidized analogues. These structural changes upon reduction reflect a net increase in C–C bond order and a net decrease in C–O bond order, in agreement with a ligand-centered reduction from ${}^{\text{R}}\text{L}^{x-}$ to ${}^{\text{R}}\text{L}^{(x+1)-\bullet}$ ($x = 2$: R = OMe, Cl, NO_2 ; $x = 0$: R = SMe_2), as has been observed for similar benzoquinoid-bridged metal complexes.^{28d,29a,b} Furthermore, the mean Fe–O bond distance of 2.052(1)–2.084(1) Å in the **2-R**-solvent series is 1.5–2.8% shorter than corresponding distances in **1-R**-solvent, and the mean intramolecular Fe···Fe distance decreases to a similar degree in moving from **1-R**-solvent to **2-R**-solvent (R = OMe, Cl, NO_2 , SMe_2). Together, these observations highlight the stronger Fe–O interactions in the radical-bridged complexes $[({\text{Me}_3\text{TPyA}})_2\text{Fe}_2({}^{\text{R}}\text{L}^{x-\bullet})]^{n+}$ ($x = 3, n = 1$: R = OMe, Cl, NO_2 ; $x = 1, n = 3$: R = SMe_2) than in the diamagnetic ligand-bridged analogues $[({\text{Me}_3\text{TPyA}})_2\text{Fe}_2({}^{\text{R}}\text{L}^{x-})]^{n+}$ ($x = 2, n = 2$: R = OMe, Cl, NO_2 ; $x = 0, n = 4$: R = SMe_2) owing to the increase in anionic charge. As a result of stronger interactions between the Fe^{II} centers and the bridging ligand in **2-R**-solvent, the average Fe–N bond distance increases slightly by 1.0–1.8% in moving from **1-R**-solvent to **2-R**-solvent (R = OMe, Cl, NO_2 , SMe_2).

Mössbauer Spectroscopy. To confirm the presence of a bridging ligand-centered reduction and further probe the effects of tetraoxolene substitution on the electronic structures of **1-R** and **2-R**, zero-field ${}^{57}\text{Fe}$ Mössbauer spectra were collected for polycrystalline samples at 80 K. The Mössbauer spectra for **1-R** exhibit a single sharp doublet (see Figure 4, top). Lorentzian fits to the data give an isomer shift of $\delta = 1.076(3)–1.111(3)$ mm s^{-1} and a quadrupole splitting of $\Delta E_Q = 2.36(2)–2.61(2)$ mm s^{-1} across the series (see Table 2). These parameters are consistent with high-spin Fe^{II} centers in

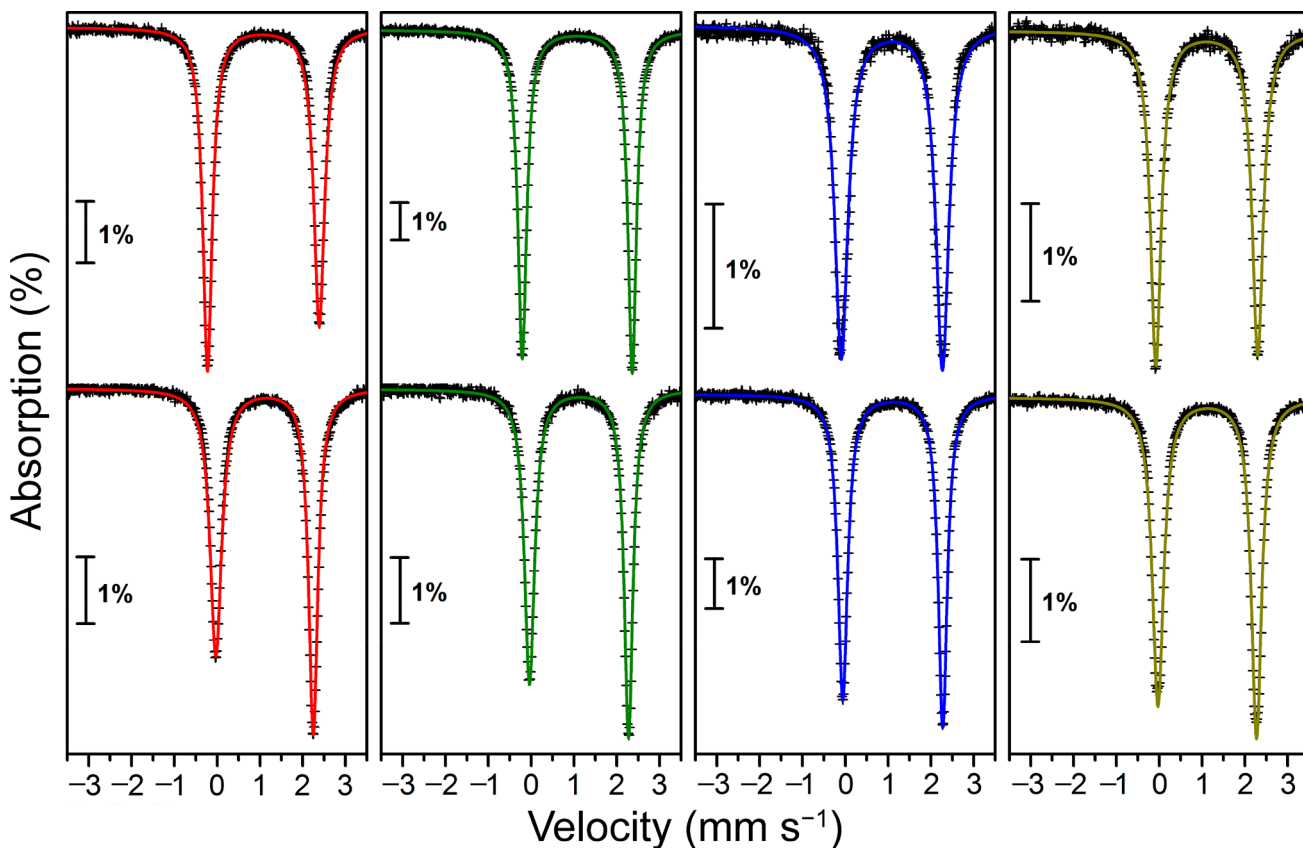


Figure 4. Zero-field ^{57}Fe Mössbauer spectra for polycrystalline samples of **1-R** (top) and **2-R** (bottom) at 80 K; R = OMe (red), Cl (green), NO_2 (blue), SMe₂ (gold). Black crosses represent experimental data, and colored lines correspond to Lorentzian fits to the data. Each vertical scale bar represents an absorption of 1%.

Table 2. Summary of Parameters Obtained from Fits to Zero-Field ^{57}Fe Mössbauer Spectra for **1-R and **2-R** at 80 K^a**

	1-OMe	2-OMe	1-Cl	2-Cl	1- NO_2	2- NO_2	1-SMe ₂	2-SMe ₂
δ (mm s ⁻¹)	1.081(3)	1.108(3)	1.076(3)	1.118(3)	1.087(3)	1.108(3)	1.111(3)	1.121(3)
ΔE_Q (mm s ⁻¹)	2.61(2)	2.28(2)	2.57(2)	2.31(2)	2.36(2)	2.33(2)	2.38(2)	2.30(2)
Γ_L^b (mm s ⁻¹)	0.263(3)	0.330(3)	0.249(2)	0.286(3)	0.371(4)	0.274(3)	0.302(4)	0.319(3)
Γ_R^c (mm s ⁻¹)	0.306(3)	0.256(3)	0.240(2)	0.243(3)	0.362(4)	0.253(3)	0.315(4)	0.291(3)

^aSee Figure 4 for the experimental data and corresponding fits using Lorentzian doublets. The uncertainties in the parameter values were estimated from a combination of experimental and statistical fitting errors as described in the Experimental Section. ^b Γ_L denotes the width of the left line of a quadrupole doublet. Γ_R denotes the width of the right line of a quadrupole doublet.

a pseudo-octahedral geometry and agree well with values reported for dinuclear complexes^{29,36,37,40,42} and extended solids⁴³ featuring Fe^{II} ions in similar coordination environments. The spectra for **2-R** display a similar quadrupole doublet (see Figure 4, bottom), with an isomer shift of $\delta = 1.108(3)-1.121(3)$ mm s⁻¹ and a quadrupole splitting of $\Delta E_Q = 2.28(2)-2.33(2)$ mm s⁻¹ for the series (see Table 2). The nearly identical isomer shifts in **1-R** and **2-R** confirm the one-electron reduction from **1-R** to **2-R** to be centered on the bridging ligand. Notably, compounds **2-R** exhibit a smaller quadrupole splitting than their corresponding oxidized analogues **1-R**. This difference is most pronounced for the OMe- and Cl-substituted derivatives (see Table 2) and likely stems from the change in ligand field at the Fe^{II} centers associated with the reduction of the bridging ligand. The slight asymmetry of the quadrupole doublet for **1-OMe** and **2-R** may be attributed to several effects, including slow spin relaxation of $S = 2$ Fe^{II} ions,⁴⁴ sample texture effects,^{44a,45} and lattice vibrational anisotropy.^{44a,45a} A complete understanding of the

origin of this asymmetry requires detailed variable-temperature analysis that is beyond the scope of this work. Overall, the foregoing Mössbauer spectroscopic analysis corroborates the assignment of the Fe₂ complexes in **1-R** as $[(\text{Me}_3\text{TPyA})_2\text{Fe}_2(\text{R}^{Lx-})]^{n+}$ ($x = 2, n = 2$: R = OMe, Cl, NO_2 ; $x = 0, n = 4$: R = SMe₂) and **2-R** as $[(\text{Me}_3\text{TPyA})_2\text{Fe}_2(\text{R}^{Lx-\bullet})]^{n+}$ ($x = 3, n = 1$: R = OMe, Cl, NO_2 ; $x = 1, n = 3$: R = SMe₂), in accord with single-crystal X-ray diffraction analysis.

UV–Vis–NIR Spectroscopy. To gain further insight into the electronic structures of **1-R** and **2-R**, UV–vis–NIR (NIR = near-infrared) absorption spectra were collected for MeCN solutions at 298 K. The spectra for all compounds show an intense absorption band centered at 261–263 nm ($\epsilon_{\max} = 28\,700-37\,700\text{ M}^{-1}\text{ cm}^{-1}$), as depicted in Figure 5. Considering the identical feature in the spectrum for Me₃TPyA (see Figure S23) and the invariance of λ_{\max} and ϵ_{\max} on the oxidation state of the bridging ligand, we assign this absorption to a $\pi-\pi^*$ transition occurring within the Me₃TPyA capping ligand.⁴⁶ The spectra for **1-R** display an additional strong band

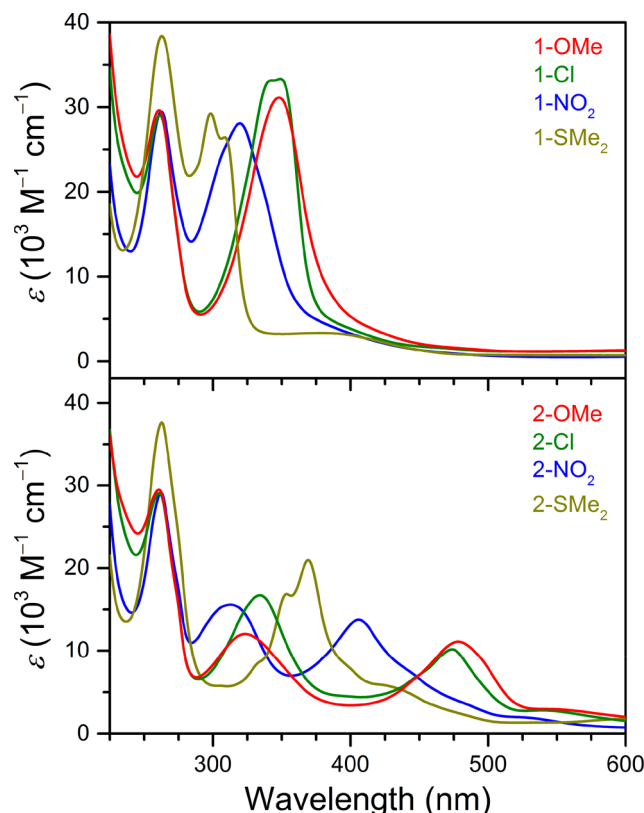


Figure 5. UV–Vis spectra for solutions of **1-R** (top) and **2-R** (bottom) in MeCN at 298 K.

in the near-UV region that exhibits a progressive bathochromic shift ($\lambda_{\text{max}} = 298\text{--}350\text{ nm}$; $\epsilon_{\text{max}} = 25\,800\text{--}34\,700\text{ M}^{-1}\text{ cm}^{-1}$) as the electron-donating ability of the substituents increases (see Figure 5, top). On the basis of the similarity with the spectra for the free ligands (see Figures S24–S27) and literature precedent for other complexes bearing quinoid ligands,⁴⁷ this band is ascribed to a $\pi\text{--}\pi^*$ transition within the bridging ligand. Notably, the spectra for **2-OMe**, **2-Cl**, and **2-NO₂** feature two broad tetraoxolene-centered $\pi\text{--}\pi^*$ bands^{28e} at $\lambda_{\text{max}} = 313\text{--}334\text{ nm}$ ($\epsilon_{\text{max}} = 12\,000\text{--}16\,700\text{ M}^{-1}\text{ cm}^{-1}$) and $\lambda_{\text{max}} = 406\text{--}478\text{ nm}$ ($\epsilon_{\text{max}} = 10\,200\text{--}13\,800\text{ M}^{-1}\text{ cm}^{-1}$) for the series, which are significantly weaker than those for the oxidized analogues (see Figure 5, bottom). In contrast, the spectrum for **2-SMe₂** exhibits a markedly different profile than those for **2-OMe**, **2-Cl**, and **2-NO₂**. Specifically, multiple overlapping tetraoxolene-centered $\pi\text{--}\pi^*$ bands are present in the 300–500 nm range, with $\lambda_{\text{max}} = 369\text{ nm}$ ($\epsilon_{\text{max}} = 21\,000\text{ M}^{-1}\text{ cm}^{-1}$). This discrepancy most likely arises from the different charges of the Fe^{II}₂ complexes in these compounds.

Close comparison of the vis–NIR region of the spectra obtained for **1-R** and **2-R** reveals that compounds **1-R** generally feature stronger absorption in the NIR region than do **2-R**, while additional bands are observed between 525 and 650 nm in the spectra for **2-R** (see Figures S28–S33). We tentatively assign these new bands to charge-transfer transitions based on the molar absorptivity values ($\epsilon_{\text{max}} = 1770\text{--}3960\text{ M}^{-1}\text{ cm}^{-1}$). Taken together, the spectral changes observed upon reduction of the bridging ligand are in good agreement with the associated color change from dark green for **1-R** to red-brown ($R = \text{OMe, Cl, NO}_2$) or green-brown ($R = \text{SMe}_2$) for **2-R**. Furthermore, these studies demonstrate that the solution electronic structures of **1-R** and **2-R** are

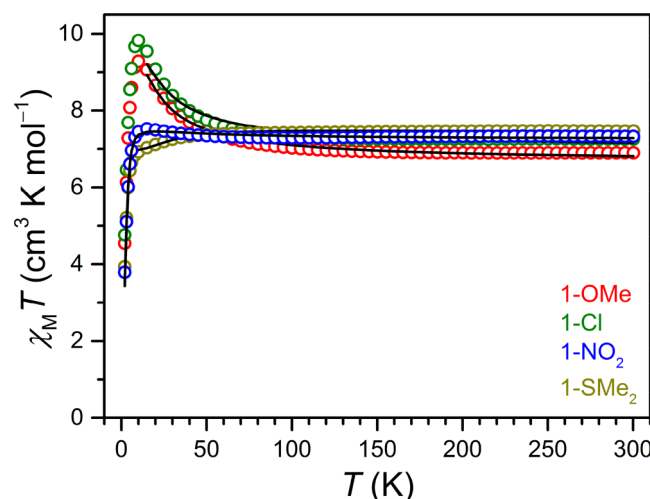


Figure 6. Variable-temperature dc magnetic susceptibility data for **1-R**, collected under an applied field of 1 T. Colored circles represent experimental data, and black lines correspond to fits to the data.

significantly affected by the nature of the substituents, although the establishment of a clear trend is complicated by broad features and differences in overall charges. Along these lines, the diffuse reflectance spectra collected for microcrystalline samples of **1-R** and **2-R** (see Figures S34–S41) show similar features as the solution spectra, suggesting that the substituents also play an important role in determining the electronic properties of these compounds in the solid state.

Static Magnetic Properties. To probe and compare magnetic interactions in **1-R** and **2-R**, variable-temperature dc magnetic susceptibility data were collected for microcrystalline samples under an applied field of 1 T. The resulting plots of $\chi_M T$ versus T for **1-R** are shown in Figure 6. At 300 K, the values of $\chi_M T = 6.90, 7.25, 7.32$, and $7.47\text{ cm}^3\text{ K mol}^{-1}$ for **1-OMe**, **1-Cl**, **1-NO₂**, and **1-SMe₂**, respectively, correspond to two magnetically noninteracting $S = 2$ Fe^{II} centers with $g = 2.14, 2.20, 2.21$, and 2.23 , respectively. As the temperature is decreased, the data for **1-OMe** and **1-Cl** undergo a gradual then rapid increase, reaching maximum values of 9.28 and $9.82\text{ cm}^3\text{ K mol}^{-1}$ at 10 K , respectively. This increase in $\chi_M T$ with decreasing temperature is indicative of weak ferromagnetic coupling between the Fe^{II} centers via a superexchange mechanism through the diamagnetic tetraoxolene ligand to give an $S = 4$ ground state. Below 10 K , $\chi_M T$ decreases sharply to minimum values of 4.54 and $4.76\text{ cm}^3\text{ K mol}^{-1}$ at 2.0 K for **1-OMe** and **1-Cl**, respectively, likely the result of Zeeman splitting, zero-field splitting, and/or weak intermolecular interactions. In contrast, the temperature dependence of $\chi_M T$ for **1-NO₂** and **1-SMe₂** is not as pronounced as observed for **1-OMe** and **1-Cl**. Rather, the $\chi_M T$ data for **1-NO₂** show a gradual increase to a maximum value of $\chi_M T = 7.52\text{ cm}^3\text{ K mol}^{-1}$ at 15 K and then undergo a sharp decline to a minimum value of $3.79\text{ cm}^3\text{ K mol}^{-1}$ at 2.0 K . Similarly, the value of $\chi_M T$ for **1-SMe₂** is relatively constant above 60 K but then decreases gradually as the temperature is decreased from 60 K , and more sharply below 10 K , to a minimum value of $3.93\text{ cm}^3\text{ K mol}^{-1}$ at 2.0 K . The different magnetic behavior observed for **1-NO₂** and **1-SMe₂** than that observed for **1-OMe** and **1-Cl** likely stems from weaker magnetic exchange interactions through diamagnetic bridging ligands bearing electron-withdrawing

Table 3. Summary of Parameters Obtained from Fits to Magnetic Data for 1-R and 2-R

	1-OMe	1-Cl	1-NO ₂	1-SMe ₂	2-OMe	2-Cl	2-NO ₂	2-SMe ₂
D (cm ⁻¹)	-4.8(4) ^a	-8.0(6) ^a	-7.0(4) ^a	-15(2) ^b	-16.9(2) ^c	-12.4(1) ^c	-20.7(3) ^c	-19.9(3) ^c
g	2.11(3) ^a	2.16(3) ^a	2.20(2) ^a	2.22(3) ^a	2.11 ^c	2.14 ^c	2.23 ^c	2.36 ^c
J (cm ⁻¹)	+1.2(2) ^a	+1.2(2) ^a	+0.3(1) ^a	+0.3(1) ^a	-57(10) ^d	-60(7) ^d	-58(6) ^d	-65(8) ^d
U _{eff} ^e (cm ⁻¹)					50(1)	41(1)	38(1)	33(1)
τ ₀ ^e (ns)					3.3(6)	10(2)	18(3)	110(30)

^aThese values were obtained from a simultaneous fit to low-temperature magnetization and dc magnetic susceptibility data, as described in the Experimental Section. ^bThis value of D was obtained from an individual fit to low-temperature magnetization data using fixed values of g and J, as described in the Experimental Section and Table S5. ^cThese values were obtained from fits to low-temperature magnetization data, as described in the Experimental Section. ^dThese values of J were obtained from fits to dc magnetic susceptibility data in the temperature range 60–300 K using the spin Hamiltonian provided in eq 3 in the Experimental Section. ^eThese values were obtained from ac magnetic susceptibility measurements collected under zero applied dc field, as described in the Experimental Section.

substituents, as has been previously observed,^{32,33} and/or larger zero-field splitting.

To assess the presence of magnetic anisotropy and confirm the spin ground states in 1-R, low-temperature magnetization data were collected at selected dc fields (see Figures S42–S45). The saturation magnetization values of the resulting isofield curves fall in the range of M = 5.26–6.37 μ_B mol⁻¹ across the series, in accord with the presence of an S = 4 ground state and significant magnetic anisotropy for all compounds.

To quantify the magnetic exchange interactions and magnetic anisotropy in 1-R, the variable-temperature dc magnetic susceptibility data and low-temperature magnetization data were simultaneously fit to the Van Vleck equation according to the spin Hamiltonian provided in eq 1 (see Experimental Section). Fits to the data give exchange constants of J = +1.2(2), +1.2(2), +0.3(1), and +0.3(1) cm⁻¹ for 1-OMe, 1-Cl, 1-NO₂, and 1-SMe₂, respectively, along with values of the axial zero-field splitting parameter D ranging from -4.8(4) to -15(2) cm⁻¹ and g = 2.11(3)–2.22(3) across the series (see Table 3). Note that the values of g obtained from these fits are in excellent agreement with those estimated from the χ_MT values at 300 K. Furthermore, the magnitude and sign of J for 1-R is consistent with other examples of benzoquinoid-bridged Fe^{II}₂ complexes.^{28d,40} Interestingly, the value of J is identical for 1-OMe and 1-Cl, and this value is 4 times larger than the value of J = +0.3(1) cm⁻¹ obtained for both 1-NO₂ and 1-SMe₂, demonstrating that strongly electron-withdrawing ligand substituents decrease the magnetic coupling strength through a diamagnetic tetraoxolene bridge. The lack of a linear correlation between J and the Hammett substituent constant σ_p for the 1-R series may be attributed to the ability of halogen substituents to donate a lone pair of electrons. Specifically, the electron-donating resonance effects may outweigh the electron-withdrawing inductive effects for the Cl substituents and thus render the electronic properties of ^{Cl}L²⁻ close to that of ^{OMe}L²⁻ when coordinated to metal ions. Indeed, the similar UV-vis absorption spectra and Mössbauer parameters obtained for 1-OMe and 1-Cl support this hypothesis. Furthermore, similar magnetic properties have been observed for paramagnetic metal complexes featuring aromatic ligands with OMe and Cl substituents.⁴⁸

The plots of χ_MT versus T for 2-R exhibit a markedly different profile than those for 1-R (see Figure 7). The values of χ_MT at 300 K are 6.10, 6.41, 6.59, and 7.00 cm³ K mol⁻¹ for 2-OMe, 2-Cl, 2-NO₂, and 2-SMe₂, respectively. As the temperature is decreased to 150 K, χ_MT undergoes a gradual increase and then increases nearly linearly upon further

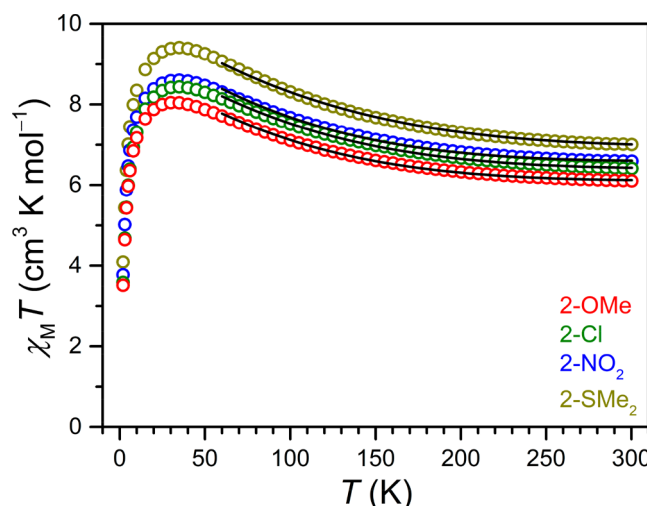


Figure 7. Variable-temperature dc magnetic susceptibility data for 2-R, collected under an applied field of 1 T. Colored circles represent experimental data, and black lines correspond to fits to the data.

decreasing the temperature to reach maximum values of 8.04, 8.44, 8.60, and 9.41 cm³ K mol⁻¹ at 30, 35, 35, and 35 K for 2-OMe, 2-Cl, 2-NO₂, and 2-SMe₂, respectively. This upturn in χ_MT with decreasing temperature suggests significant magnetic coupling between the two Fe^{II} centers and semi-quinoid radical ligand via a direct exchange mechanism. To quantify this interaction and to determine whether it is ferromagnetic or antiferromagnetic in nature, the data were fit in the temperature range of 60–300 K to the Van Vleck equation according to the spin Hamiltonian provided in eq 3 (see Experimental Section) to give exchange constants of J = -57(10), -60(7), -58(6), and -65(8) cm⁻¹ for 2-OMe, 2-Cl, 2-NO₂, and 2-SMe₂, respectively (see Table 3), with g = 2.09(4), 2.14(3), 2.17(3), 2.23(4), respectively. Note that the introduction of an Fe^{II}...Fe^{II} superexchange coupling term in the spin Hamiltonian does not significantly affect the metal–radical exchange coupling constants (see Table S6). Interestingly, the antiferromagnetic coupling in 2-Cl is in contrast to the ferromagnetic coupling (J = +19 cm⁻¹) for the related complex [(TPyA)₂Fe^{II}₂(^{Cl}L^{3-•})]⁺.^{28d} This drastically different magnetic behavior may stem from structural differences imposed by the bulkier Me₃TPyA capping ligand in 2-R; however, the lack of a crystal structure for [(TPyA)₂Fe^{II}₂(^{Cl}L^{3-•})]⁺ precludes further insight.

The rapid decline in χ_MT below 30 K can be attributed to Zeeman splitting, zero-field splitting, and/or weak intermolecular interactions. Indeed, low-temperature magnetization

data for **2-R** reveal the presence of substantial zero-field splitting, with fits to the data giving values of $D = -16.9(2)$, $-12.4(1)$, $-20.7(3)$, and $-19.9(3) \text{ cm}^{-1}$ for **2-OMe**, **2-Cl**, **2-NO₂**, and **2-SMe₂**, respectively, and $g = 2.11$, 2.14 , 2.23 , 2.36 , respectively (see Figures S46–S49 and Tables 3 and S7–S10). Note that the values of g obtained from the low-temperature magnetization data agree well with those obtained from the variable-temperature dc susceptibility data. Interestingly, for both the **1-R** and **2-R** series of compounds, the value of g follows the trend $\text{R} = \text{OMe} < \text{Cl} < \text{NO}_2 < \text{SMe}_2$. This increase in g across the series may stem from increasing electron-withdrawing ability of the substituents, although we note that other effects, such as those arising from crystal packing, cannot be ruled out.

The values of J for **2-R** represent 48–217-fold increases from those observed for the **1-R** series (see Table 3), demonstrating the much stronger Fe^{II}–radical direct exchange coupling than Fe^{II}–Fe^{II} superexchange coupling, similar to previous observations for dinuclear benzoquinoid-bridged complexes.^{28d,29a,b} However, the substituents bear a remarkably insignificant effect on the magnitude of metal–radical coupling in **2-R**. This is in contrast with the clearly distinct $\chi_M T$ versus T profiles and values of J for $\text{R} = \text{OMe}$, Cl and $\text{R} = \text{NO}_2$, SMe_2 , observed for the **1-R** series. These results suggest that the effects of ligand substituents on magnetic coupling strength in tetraoxolene-bridged complexes are highly dependent on the oxidation state of the bridging ligand. Accordingly, the contributions from substituents to ligand-based orbitals that mediate magnetic coupling between paramagnetic metal centers through a diamagnetic bridge are likely significantly greater than such contributions to the ligand-based magnetic orbital of radical states. This discrepancy may be attributed to the more favorable donation of electron density into the diamagnetic ring than into the radical ring, owing to the greater negative charge and electron delocalization in the latter.

Density Functional Theory Calculations. To provide greater insight into the effects of ligand substitution on J in **1-R** and **2-R**, broken-symmetry density functional theory (DFT) calculations were performed. The possible spin couplings were explored by calculating $M_S = 4$ and $M_S = 0$ determinants for the **1-R** series and $M_S = 9/2$, $7/2$, and $1/2$ determinants for the **2-R** series. The DFT energies reveal a small energy difference between the $M_S = 4$ and $M_S = 0$ spin states and weak magnetic coupling for **1-R** (see Table S11) that are consistent with the small values of J obtained from magnetic measurements, albeit the sign is not correctly predicted for all compounds, likely stemming from the weak interactions. In contrast, computations reveal that the $M_S = 7/2$ spin state is lowest in energy for all members of the **2-R** series, and the calculated exchange constants of $J = -58$ to -85 cm^{-1} are in good agreement with experimental values (see Table S12).

The computed spin density distributions ($M_S = 4$ solution for **1-R** and $M_S = 7/2$ solution for **2-R**) show that, for both series of Fe₂ complexes, the substituents at the 3- and 6-positions on the bridging ligand do not contribute significantly to the magnetic orbitals (see Figures 8 and S53–S55). The analogous α -spin densities localized on the coordinating O atoms and Fe atoms in **1-OMe** and **1-Cl** are consistent with identical values of J for these compounds (see Figures 8, top, and S50 and Tables S13 and S14). Furthermore, the smaller α -spin densities on the four O donors in **1-NO₂** and **1-SMe₂** (see Figures S51 and S52 and Tables S15 and S16) are in accord with weaker ferromagnetic coupling in **1-NO₂** and **1-SMe₂**.

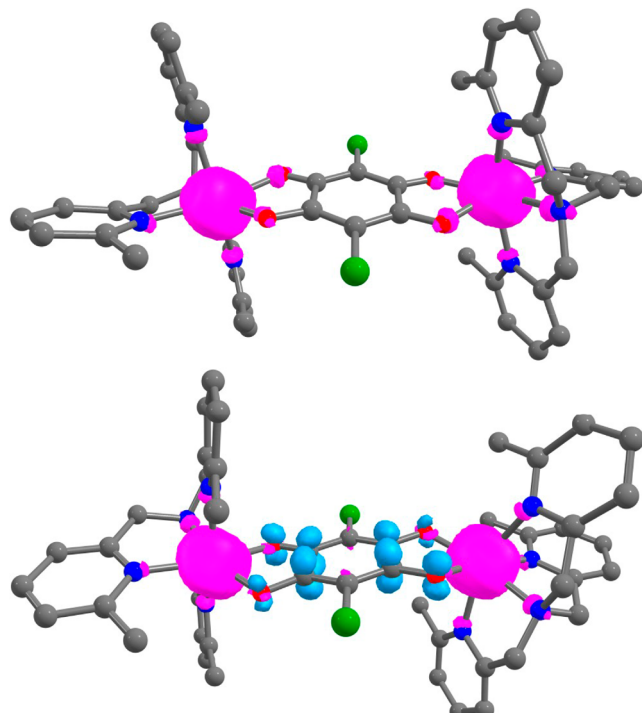


Figure 8. Calculated spin densities for **1-Cl** (top) and **2-Cl** (bottom) shown at 0.01 isovalue with α -spin in magenta and β -spin in cyan. Green, red, blue, and gray spheres represent Cl, O, N, and C atoms, respectively; H atoms and $(\text{BF}_4)^-$ anions are omitted for clarity. Calculations were performed on the high-spin $M_S = 4$ and the lowest-energy $M_S = 7/2$ broken-symmetry solutions for **1-Cl** and **2-Cl**, respectively, using the experimental single-crystal X-ray structure geometries. See Supporting Information for analogous spin densities for other complexes.

than in **1-OMe** and **1-Cl**. The presence of large β -spin densities on the coordinating O atoms and the four C atoms on the tetraoxolene ring to which they are attached in **2-R** are consistent with stronger magnetic coupling in the radical-bridged Fe^{II}₂ complexes that is antiferromagnetic in nature (see Figures 8, bottom, and S53–S55 and Tables S17–S20). The β -spin density is distributed over all four O donor atoms in **2-NO₂** and **2-SMe₂**, whereas the spin density is largely localized on one set of O atoms in **2-OMe** and **2-Cl**, suggesting different dominant exchange pathways within the series. Nevertheless, the computed spin densities for **2-R** are in accord with the minimal impact of bridging ligand substitution on the magnetic coupling strength, as negligible spin density is located on the substituents and the C atoms to which they are bonded.

Inspection of the molecular orbitals further supports the insignificant effects of ligand substitution on the value of J for **2-R**. The molecular orbital energy-level diagrams (see Figures S56–S63) for **1-R** and **2-R** reveal that the unpaired electron on the radical bridging ligand in **2-R** occupies a bonding β -spin π orbital that has negligible contribution from the substituents and the associated C atoms of the ring (see Figures S64–S67). These results are in accord with those obtained for free $\text{Cl}_3^{\cdot-}$.^{28e} Because the overlap between this ligand-based π orbital and Fe-based t_{2g} orbitals predominantly determines the magnitude of the exchange coupling in these compounds, the nature of the bridging ligand substituents should have minimal effect. Moreover, analysis of spin density distributions in related mono- and dinuclear transition-metal complexes

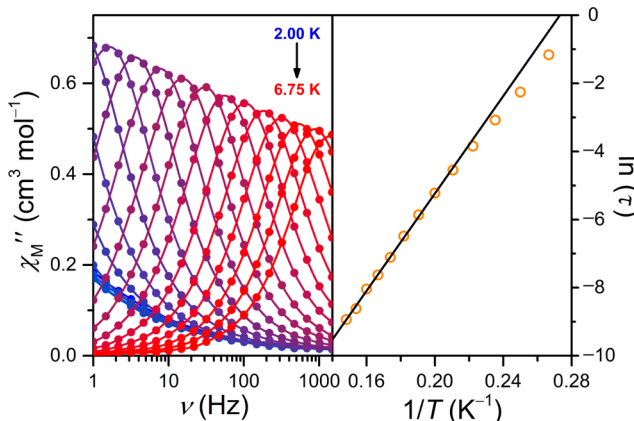


Figure 9. Variable-frequency out-of-phase ac susceptibility data for **2-OMe**, collected under zero applied dc field in the temperature range of 2.00–6.75 K (left), and corresponding Arrhenius plot of relaxation time (right). Colored lines are a guide to the eye, and the black line corresponds to a linear fit to the data.

featuring terminal or bridging semiquinone, iminosemiquinone, and diiminosemiquinone radical ligands and Fe^{III} ⁴⁹, Co^{III} ⁵⁰, Ni^{II} ⁵¹, Ru^{II} ⁵², and Pt^{II} ⁵³ metal centers of different geometries reveals similar insignificant contribution from the substituents at 3- and 6-positions on the quinoid ring to the total spin density.⁵⁴ This suggests that the minimal influence of the ring-bound substituents on magnetic coupling strength may not be limited to tetraoxolene-bridged Fe^{II}_2 complexes, as observed in **2-R**, but could generally apply to metal-semiquinoid compounds.

Dynamic Magnetic Properties. Finally, the presence of large negative values of D for **1-R** and **2-R** prompted us to probe potential slow magnetic relaxation in these compounds. Accordingly, variable-frequency ac magnetic susceptibility data were collected under zero applied dc field in the temperature range of 2.00–8.00 K. For **1-R**, only onsets of peaks in the out-of-phase component (χ_M'') of the ac susceptibility were observed above 2.00 K and below 1488 Hz, indicating too fast magnetic relaxation (see Figures S68–S75). In stark contrast, compounds **2-R** exhibit pronounced temperature- and frequency-dependent peaks in both the in-phase (χ_M') and out-of-phase component (χ_M'') of the ac susceptibility (see Figures 9, left, and S76–S90), which demonstrates that the radical-bridged complexes are indeed single-molecule magnets. These data were employed to construct Cole–Cole plots (see Figures S91, S92, S94, and S96), which were fit using the generalized Debye model⁵⁵ to estimate relaxation times (τ). The corresponding Arrhenius plots of relaxation time exhibit linear regions at higher temperatures between 4.75 and 6.75 K, between 4.75 and 6.50 K, between 4.25 and 6.25 K, and between 5.50 and 7.00 K for **2-OMe**, **2-Cl**, **2-NO₂**, and **2-SMe₂**, respectively (see Figures 9, right, S93, S95, and S97), indicating a thermally activated relaxation process for all complexes. Fits to the data in these temperature ranges afford spin relaxation barriers of $U_{\text{eff}} = 50(1)$, $41(1)$, $38(1)$, and $33(1)$ cm^{-1} for **2-OMe**, **2-Cl**, **2-NO₂**, and **2-SMe₂**, respectively, with corresponding pre-exponential factors of $\tau_0 = 3.3(6) \times 10^{-9}$, $1.0(2) \times 10^{-8}$, $1.8(3) \times 10^{-8}$, and $1.1(3) \times 10^{-7}$ s (see Table 3). These values are similar to those obtained for related tetraazalene-bridged Fe^{II}_2 complexes.^{29a,b} Interestingly, the plot of U_{eff} versus the Hammett substituent constant σ_p for the series **2-R** reveals a linear relationship (see Figure

S98). Note, however, that this ostensible substituent dependence of U_{eff} is complicated by a nonconstant τ_0 across the series, which influences U_{eff} . Alternatively, inspection of the relaxation time τ across the series at 2.00, 4.00, and 6.00 K reveals the absence of a discernible trend (see Figures S99–S101). As such, the data reported here do not conclusively show the relaxation dynamics of **2-R** to be dependent on tetraoxolene substitution.

At lower temperatures, the data begin to deviate from linearity and finally reach a plateau below 3.00, 2.75, and 4.00 K for **2-Cl**, **2-NO₂**, and **2-SMe₂**, respectively, suggesting the presence of additional fast relaxation processes, such as quantum tunneling and/or spin–spin relaxation, that shortcut the energy barrier. These additional relaxation processes are most prominent for **2-SMe₂**, as the temperature-dependent features in the plot of χ_M'' versus ν are observed at much higher frequencies than those for **2-OMe**, **2-Cl**, and **2-NO₂**. This discrepancy may arise from the different charges of the Fe^{II}_2 complexes in these compounds and/or the steric bulk of the $^+\text{SMe}_2$ groups.

CONCLUSIONS AND OUTLOOK

The foregoing results demonstrate the insignificant effects of ligand substitution on the metal–radical exchange coupling in tetraoxolene radical-bridged Fe^{II}_2 complexes. Moving from $R = \text{OMe}$ or Cl to $R = \text{NO}_2$ or SMe_2 in the Fe_2 complexes featuring the diamagnetic form of the bridging ligand leads to a decrease in coupling strength from $J = +1.2(2)$ cm^{-1} to $J = +0.3(1)$ cm^{-1} . In stark contrast, the one-electron-reduced, radical-bridged complexes exhibit exchange coupling constants of $J = -57(10)$, $-60(7)$, $-58(6)$, and $-65(8)$ cm^{-1} for $R = \text{OMe}$, Cl , NO_2 , and SMe_2 , respectively. This insensitivity of J on ligand substitution is rationalized through electronic structure calculations, which show minimal spin density on R and the associated C atoms of the tetraoxolene ring. This systematic investigation suggests that substitution of the 3- and 6-positions of quinoid bridging ligands is not an effective strategy to increase metal–radical coupling. Rather, selection of ligand substituents should perhaps be based on considerations such as synthetic accessibility of the ligand itself or of the resulting metal compound, or the potential of the substituent to impart secondary function such as conductivity or photophysical properties.

ASSOCIATED CONTENT

SI Supporting Information

The Supporting Information is available free of charge at <https://pubs.acs.org/doi/10.1021/acs.inorgchem.9b03736>.

Additional experimental details, characterization data, and computational data for **1-R** and **2-R** ($R = \text{OMe}$, Cl , NO_2 , SMe_2), including crystallographic data for **1-OMe**·4.0MeCN, **1-Cl**·0.7H₂O, **1-NO₂**·4.0MeCN, **1-SMe₂**·4.0MeCN, **2-OMe**·2.0MeCN, **2-Cl**·0.5Et₂O, **2-NO₂**, and **2-SMe₂**·0.9MeCN·0.5Et₂O (PDF)

Accession Codes

CCDC 1926459–1926466 contain the supplementary crystallographic data for this paper. These data can be obtained free of charge via www.ccdc.cam.ac.uk/data_request/cif, or by emailing data_request@ccdc.cam.ac.uk, or by contacting The Cambridge Crystallographic Data Centre, 12 Union Road, Cambridge CB2 1EZ, UK; fax: +44 1223 336033.

AUTHOR INFORMATION

Corresponding Author

T. David Harris – Department of Chemistry, Northwestern University, Evanston 60208, Illinois, United States; Department of Chemistry, University of California, Berkeley 94720, California, United States;  orcid.org/0000-0003-4144-900X; Email: dharris@berkeley.edu

Authors

Agnes E. Thorarinsdottir – Department of Chemistry, Northwestern University, Evanston 60208, Illinois, United States;  orcid.org/0000-0001-9378-4454

Ragnar Bjornsson – Department of Inorganic Spectroscopy, Max-Planck-Institut für Chemische Energiekonversion, Mülheim an der Ruhr 45470, Germany;  orcid.org/0000-0003-2167-8374

Complete contact information is available at:
<https://pubs.acs.org/10.1021/acs.inorgchem.9b03736>

Notes

The authors declare no competing financial interest.

ACKNOWLEDGMENTS

This work was supported by the Department of Energy (DE-SC0019356). X-ray crystallography, NMR spectroscopy, and IR spectroscopy were performed at the Integrated Molecular Structure Education and Research Center at Northwestern Univ., which has received support from the Soft and Hybrid Nanotechnology Experimental Resource (NSF NNCI-1542205), the State of Illinois, and the International Institute for Nanotechnology. Quantitative analysis of Fe was performed at the Northwestern Univ. Quantitative Bio-element Imaging Center. Quantum chemical calculations were performed at a computing cluster at the Max Planck Institute for Chemical Energy Conversion. We thank Mr. B. D. Coleman, Dr. D. Z. Zee, Dr. J. P. S. Walsh, and Ms. Y. Wang for experimental assistance and helpful discussions. R. B. thanks the Max Planck Society for support.

REFERENCES

- (1) (a) Caneschi, A.; Gatteschi, D.; Sessoli, R.; Barra, A. L.; Brunel, L. C.; Guillot, M. Alternating Current Susceptibility, High Field Magnetization, and Millimeter Band EPR Evidence for a Ground $S = 10$ State in $[\text{Mn}_{12}\text{O}_{12}(\text{CH}_3\text{COO})_{16}(\text{H}_2\text{O})_4] \cdot 2\text{CH}_3\text{COOH} \cdot 4\text{H}_2\text{O}$. *J. Am. Chem. Soc.* **1991**, *113*, 5873–5874. (b) Sessoli, R.; Gatteschi, D.; Caneschi, A.; Novak, M. A. Magnetic Bistability in a Metal-Ion Cluster. *Nature* **1993**, *365*, 141–143. (c) Sessoli, R.; Tsai, H.-L.; Schake, A. R.; Wang, S.; Vincent, J. B.; Folting, K.; Gatteschi, D.; Christou, G.; Hendrickson, D. N. High-Spin Molecules: $[\text{Mn}_{12}\text{O}_{12}(\text{O}_2\text{CR})_{16}(\text{H}_2\text{O})_4]$. *J. Am. Chem. Soc.* **1993**, *115*, 1804–1816. (d) Ishikawa, N.; Sugita, M.; Ishikawa, T.; Koshihara, S.-Y.; Kaizu, Y. Lanthanide Double-Decker Complexes Functioning as Magnets at the Single-Molecular Level. *J. Am. Chem. Soc.* **2003**, *125*, 8694–8695. (e) Berlinguette, C. P.; Vaughn, D.; Cañada-Vilalta, C.; Galán-Mascarós, J. R.; Dunbar, K. R. A Trigonal-Bipyramidal Cyanide Cluster with Single-Molecule-Magnet Behavior: Synthesis, Structure, and Magnetic Properties of $\{[\text{Mn}^{\text{II}}(\text{tmpphen})_2]_3[\text{Mn}^{\text{III}}(\text{CN})_6]_2\}$. *Angew. Chem., Int. Ed.* **2003**, *42*, 1523–1526. (f) Tang, J.; Hewitt, I.; Madhu, N. T.; Chastanet, G.; Wernsdorfer, W.; Anson, C. E.; Benelli, C.; Sessoli, R.; Powell, A. K. Dysprosium Triangles Showing Single-Molecule Magnet Behavior of Thermally Excited Spin States. *Angew. Chem., Int. Ed.* **2006**, *45*, 1729–1733. (g) Gatteschi, D.; Sessoli, R.; Villain, J. *Molecular Nanomagnets*; Oxford University Press: Oxford, UK, 2006. (h) *Single-Molecule Magnets and Related Phenomena. Structure and Bonding*; Winpenny, R. E. P., Ed.; Springer-Verlag: Berlin, Germany, 2006; Vol. 122, pp 1–161.

(i) Lin, P.-H.; Burchell, T. J.; Clérac, R.; Murugesu, M. Dinuclear Dysprosium(III) Single-Molecule Magnets with a Large Anisotropic Barrier. *Angew. Chem., Int. Ed.* **2008**, *47*, 8848–8851. (j) Bagai, R.; Christou, G. The *Drosophila* of Single-Molecule Magnetism: $[\text{Mn}_{12}\text{O}_{12}(\text{O}_2\text{CR})_{16}(\text{H}_2\text{O})_4]$. *Chem. Soc. Rev.* **2009**, *38*, 1011–1026. (k) Freedman, D. E.; Harman, W. H.; Harris, T. D.; Long, G. J.; Chang, C. J.; Long, J. R. Slow Magnetic Relaxation in a High-Spin Iron(II) Complex. *J. Am. Chem. Soc.* **2010**, *132*, 1224–1225. (l) Rinehart, J. D.; Fang, M.; Evans, W. J.; Long, J. R. Strong Exchange and Magnetic Blocking in N_2^{3-} -Radical-Bridged Lanthanide Complexes. *Nat. Chem.* **2011**, *3*, 538–542. (m) Rinehart, J. D.; Fang, M.; Evans, W. J.; Long, J. R. A N_2^{3-} Radical-Bridged Terbium Complex Exhibiting Magnetic Hysteresis at 14 K. *J. Am. Chem. Soc.* **2011**, *133*, 14236–14239. (n) Mougel, V.; Chatelain, L.; Pécaut, J.; Caciuffo, R.; Colineau, E.; Griveau, J.-C.; Mazzanti, M. Uranium and Manganese Assembled in a Wheel-Shaped Nanoscale Single-Molecule Magnet with High Spin-Reversal Barrier. *Nat. Chem.* **2012**, *4*, 1011–1017. (o) Ganivet, C. R.; Ballesteros, B.; de la Torre, G.; Clemente-Juan, J. M.; Coronado, E.; Torres, T. Influence of Peripheral Substitution on the Magnetic Behavior of Single-Ion Magnets Based on Homo- and Heteroleptic Tb^{III} Bis(phthalocyaninate). *Chem. - Eur. J.* **2013**, *19*, 1457–1465. (p) Woodruff, D. N.; Winpenny, R. E. P.; Layfield, R. A. Lanthanide Single-Molecule Magnets. *Chem. Rev.* **2013**, *113*, 5110–5148. (q) Zhang, P.; Guo, Y.-N.; Tang, J. Recent Advances in Dysprosium-Based Single Molecule Magnets: Structural Overview and Synthetic Strategies. *Coord. Chem. Rev.* **2013**, *257*, 1728–1763. (r) Pedersen, K. S.; Bendix, J.; Clérac, R. Single-Molecule Magnet Engineering: Building-Block Approaches. *Chem. Commun.* **2014**, *50*, 4396–4415. (s) Meihaus, K. R.; Long, J. R. Actinide-Based Single-Molecule Magnets. *Dalton Trans.* **2015**, *44*, 2517–2528. (t) Craig, G. A.; Murrie, M. 3d Single-Ion Magnets. *Chem. Soc. Rev.* **2015**, *44*, 2135–2147. (u) Demir, S.; Jeon, I.-R.; Long, J. R.; Harris, T. D. Radical Ligand-Containing Single-Molecule Magnets. *Coord. Chem. Rev.* **2015**, *289*–290, 149–176. (v) Chen, Y.-C.; Liu, J.-L.; Ungur, L.; Liu, J.; Li, Q.-W.; Wang, L.-F.; Ni, Z.-P.; Chibotaru, L. F.; Chen, X.-M.; Tong, M.-L. Symmetry-Supported Magnetic Blocking at 20 K in Pentagonal Bipyramidal Dy(III) Single-Ion Magnets. *J. Am. Chem. Soc.* **2016**, *138*, 2829–2837. (w) Liu, J.; Chen, Y.-C.; Liu, J.-L.; Vieru, V.; Ungur, L.; Jia, J.-H.; Chibotaru, L. F.; Lan, Y.; Wernsdorfer, W.; Gao, S.; Chen, X.-M.; Tong, M.-L. A Stable Pentagonal Bipyramidal Dy(III) Single-Ion Magnet with a Record Magnetization Reversal Barrier over 1000 K. *J. Am. Chem. Soc.* **2016**, *138*, 5441–5450. (x) Ding, Y.-S.; Chilton, N. F.; Winpenny, R. E. P.; Zheng, Y.-Z. On Approaching the Limit of Molecular Magnetic Anisotropy: A Near-Perfect Pentagonal Bipyramidal Dysprosium(III) Single-Molecule Magnet. *Angew. Chem., Int. Ed.* **2016**, *55*, 16071–16074. (y) Guo, F.-S.; Day, B. M.; Chen, Y.-C.; Tong, M.-L.; Mansikkamäki, A.; Layfield, R. A. A Dysprosium Metallocene Single-Molecule Magnet Functioning at the Axial Limit. *Angew. Chem., Int. Ed.* **2017**, *56*, 11445–11449. (z) Demir, S.; Gonzalez, M. I.; Darago, L. E.; Evans, W. J.; Long, J. R. Giant Coercivity and High Magnetic Blocking Temperatures for N_2^{3-} Radical-Bridged Dilanthanide Complexes Upon Ligand Dissociation. *Nat. Commun.* **2017**, *8*, 2144. (α) Randall McClain, K.; Gould, C. A.; Chakarawet, K.; Teat, S. J.; Groshens, T. J.; Long, J. R.; Harvey, B. G. High-Temperature Magnetic Blocking and Magneto-Structural Correlations in a Series of Dysprosium(III) Metallocenium Single-Molecule Magnets. *Chem. Sci.* **2018**, *9*, 8492–8503. (β) Albold, U.; Bamberger, H.; Hallmen, P. P.; van Slageren, J.; Sarkar, B. Strong Exchange Couplings Drastically Slow Down Magnetization Relaxation in an Air-Stable Cobalt(II)-Radical Single-Molecule Magnet (SMM). *Angew. Chem., Int. Ed.* **2019**, *58*, 9802–9806.

- (2) (a) Caneschi, A.; Gatteschi, D.; Lalio, N.; Sangregorio, C.; Sessoli, R.; Venturi, G.; Vindigni, A.; Rettori, A.; Pini, M. G.; Novak, M. A. Cobalt(II)-Nitronyl Nitroxide Chains as Molecular Magnetic Nanowires. *Angew. Chem., Int. Ed.* **2001**, *40*, 1760–1763. (b) Clérac, R.; Miyasaka, H.; Yamashita, M.; Coulon, C. Evidence for Single-Chain Magnet Behavior in a $\text{Mn}^{\text{III}}-\text{Ni}^{\text{II}}$ Chain Designed with High

- Spin Magnetic Units: A Route to High Temperature Metastable Magnets. *J. Am. Chem. Soc.* **2002**, *124*, 12837–12844. (c) Lescouëzec, R.; Vaissermann, J.; Ruiz-Pérez, C.; Lloret, F.; Carrasco, R.; Julve, M.; Verdaguer, M.; Dromzee, Y.; Gatteschi, D.; Wernsdorfer, W. Cyanide-Bridged Iron(III)–Cobalt(II) Double Zigzag Ferromagnetic Chains: Two New Molecular Magnetic Nanowires. *Angew. Chem., Int. Ed.* **2003**, *42*, 1483–1486. (d) Ferbinteanu, M.; Miyasaka, H.; Wernsdorfer, W.; Nakata, K.; Sugiura, K.-I.; Yamashita, M.; Coulon, C.; Clérac, R. Single-Chain Magnet (NEt_4) $[\text{Mn}_2(\text{S}-\text{MeOsalen})_2\text{Fe}(\text{CN})_6]$ Made of $\text{Mn}^{\text{III}}-\text{Fe}^{\text{III}}-\text{Mn}^{\text{III}}$ Trinuclear Single-Molecule Magnet with an $S_T = \frac{9}{2}$ Spin Ground State. *J. Am. Chem. Soc.* **2005**, *127*, 3090–3099. (e) Bogani, L.; Sangregorio, C.; Sessoli, R.; Gatteschi, D. Molecular Engineering for Single-Chain-Magnet Behavior in a One-Dimensional Dysprosium–Nitronyl Nitroxide Compound. *Angew. Chem., Int. Ed.* **2005**, *44*, 5817–5821. (f) Bernot, K.; Bogani, L.; Caneschi, A.; Gatteschi, D.; Sessoli, R. A Family of Rare-Earth-Based Single Chain Magnets: Playing with Anisotropy. *J. Am. Chem. Soc.* **2006**, *128*, 7947–7956. (g) Xu, H.-B.; Wang, B.-W.; Pan, F.; Wang, Z.-M.; Gao, S. Stringing Oxo-Centered Trinuclear $[\text{Mn}^{\text{III}}_3\text{O}]$ Units into Single-Chain Magnets with Formate or Azide Linkers. *Angew. Chem., Int. Ed.* **2007**, *46*, 7388–7392. (h) Ishii, N.; Okamura, Y.; Chiba, S.; Nogami, T.; Ishida, T. Giant Coercivity in a One-Dimensional Cobalt–Radical Coordination Magnet. *J. Am. Chem. Soc.* **2008**, *130*, 24–25. (i) Miyasaka, H.; Julve, M.; Yamashita, M.; Clérac, R. Slow Dynamics of the Magnetization in One-Dimensional Coordination Polymers: Single-Chain Magnets. *Inorg. Chem.* **2009**, *48*, 3420–3437. (j) Visinescu, D.; Madalan, A. M.; Andruh, M.; Duhayon, C.; Sutter, J.-P.; Ungur, L.; Van den Heuvel, W.; Chibotaru, L. F. First Heterotrimetallic $\{3\text{d}-4\text{d}-4\text{f}\}$ Single Chain Magnet, Constructed from Anisotropic High-Spin Heterometallic Nodes and Paramagnetic Spacers. *Chem. - Eur. J.* **2009**, *15*, 11808–11814. (k) Harris, T. D.; Bennett, M. V.; Clérac, R.; Long, J. R. $[\text{ReCl}_4(\text{CN})_2]^{2-}$: A High Magnetic Anisotropy Building Unit Giving Rise to the Single-Chain Magnets $(\text{DMF})_4\text{MReCl}_4(\text{CN})_2$ ($\text{M} = \text{Mn}$, Fe, Co, Ni). *J. Am. Chem. Soc.* **2010**, *132*, 3980–3988. (l) Sun, H.-L.; Wang, Z.-M.; Gao, S. Strategies Towards Single-Chain Magnets. *Coord. Chem. Rev.* **2010**, *254*, 1081–1100. (m) Feng, X.; Harris, T. D.; Long, J. R. Influence of Structure on Exchange Strength and Relaxation Barrier in a Series of $\text{Fe}^{\text{II}}\text{Re}^{\text{IV}}(\text{CN})_2$ Single-Chain Magnets. *Chem. Sci.* **2011**, *2*, 1688–1694. (n) Hoshino, N.; Iijima, F.; Newton, G. N.; Yoshida, N.; Shiga, T.; Nojiri, H.; Nakao, A.; Kumai, R.; Murakami, Y.; Oshio, H. Three-Way Switching in a Cyanide-Bridged $[\text{CoFe}]$ Chain. *Nat. Chem.* **2012**, *4*, 921–926. (o) Zhang, W.-X.; Ishikawa, R.; Breedlove, B.; Yamashita, M. Single-Chain Magnets: Beyond the Glauber Model. *RSC Adv.* **2013**, *3*, 3772–3798. (p) Vaz, M. G. F.; Cassaro, R. A. A.; Akpinar, H.; Schlueter, J. A.; Lahti, P. M.; Novak, M. A. A Cobalt Pyrenylnitronylnitroxide Single-Chain Magnet with High Coercivity and Record Blocking Temperature. *Chem. - Eur. J.* **2014**, *20*, 5460–5467. (q) Mougel, V.; Chatelain, L.; Hermle, J.; Caciuffo, R.; Colineau, E.; Tuna, F.; Magnani, N.; de Geyer, A.; Pécaut, J.; Mazzanti, M. A Uranium-Based $\text{UO}_2^{+}-\text{Mn}^{2+}$ Single-Chain Magnet Assembled Through Cation–Cation Interactions. *Angew. Chem., Int. Ed.* **2014**, *53*, 819–823. (r) Chatelain, L.; Tuna, F.; Pécaut, J.; Mazzanti, M. A Zig-Zag Uranyl(V)–Mn(II) Single Chain Magnet with a High Relaxation Barrier. *Chem. Commun.* **2015**, *51*, 11309–11312. (s) Cassaro, R. A. A.; Reis, S. G.; Araujo, T. S.; Lahti, P. M.; Novak, M. A.; Vaz, M. G. F. A Single-Chain Magnet with a Very High Blocking Temperature and a Strong Coercive Field. *Inorg. Chem.* **2015**, *54*, 9381–9383. (t) Wei, R.-M.; Cao, F.; Li, J.; Yang, L.; Han, Y.; Zhang, X.-L.; Zhang, Z.; Wang, X.-Y.; Song, Y. Single-Chain Magnets Based on Octacyanotungstate with the Highest Energy Barriers for Cyanide Compounds. *Sci. Rep.* **2016**, *6*, 24372. (u) Jiang, W.; Jiao, C.; Meng, Y.; Zhao, L.; Liu, Q.; Liu, T. Switching Single Chain Magnet Behavior via Photoinduced Bidirectional Metal-to-Metal Charge Transfer. *Chem. Sci.* **2018**, *9*, 617–622. (v) Drahoš, B.; Herchel, R.; Trávníček, Z. Single-Chain Magnet Based on 1D Polymeric Azido-Bridged Seven-Coordinate Fe(II) Complex with a Pyridine-Based Macroyclic Ligand. *Inorg. Chem.* **2018**, *57*, 12718–12726. (w) DeGayner, J. A.; Wang, K.; Harris, T. D. A Ferric Semiquinoid Single-Chain Magnet via Thermally-Switchable Metal–Ligand Electron Transfer. *J. Am. Chem. Soc.* **2018**, *140*, 6550–6553. (3) (a) Kahn, O.; Pei, Y.; Verdaguer, M.; Renard, J. P.; Sletten, J. Magnetic Ordering of $\text{Mn}^{\text{II}}\text{Cu}^{\text{II}}$ Bimetallic Chains: Design of a Molecular-Based Ferromagnet. *J. Am. Chem. Soc.* **1988**, *110*, 782–789. (b) Pereira, C. L. M.; Pedroso, E. F.; Doriguetto, A. C.; Ellena, J. A.; Boubeker, K.; Filali, Y.; Journaux, Y.; Novak, M. A.; Stumpf, H. O. Design of 1D and 2D Molecule-Based Magnets with the Ligand 4,5-Dimethyl-1,2-phenylenebis(oxamato). *Dalton Trans.* **2011**, *40*, 746–754. (4) (a) Miller, J. S.; Calabrese, J. C.; Epstein, A. J.; Bigelow, R. W.; Zhang, J. H.; Reiff, W. M. Ferromagnetic Properties of One-Dimensional Decamethylferrocenium Tetracyanoethylenide (1:1): $[\text{Fe}(\eta^5\text{-C}_5\text{Me}_5)_2]^{+}[\text{TCNE}]^{-}$. *J. Chem. Soc., Chem. Commun.* **1986**, 1026–1028. (b) Manriquez, J. M.; Yee, G. T.; McLean, R. S.; Epstein, A. J.; Miller, J. S. A Room-Temperature Molecular/Organic-Based Magnet. *Science* **1991**, *252*, 1415–1417. (c) Pokhodnya, K. I.; Bonner, M.; Her, J.-H.; Stephens, P. W.; Miller, J. S. Magnetic Ordering ($T_c = 90$ K) Observed for Layered $[\text{Fe}^{\text{II}}(\text{TCNE}^-)(\text{NCMe})_2]^+[\text{Fe}^{\text{III}}\text{Cl}_4]^-$ (TCNE = Tetracyanoethylene). *J. Am. Chem. Soc.* **2006**, *128*, 15592–15593. (d) Miller, J. S. Magnetically Ordered Molecule-Based Assemblies. *Dalton Trans.* **2006**, 2742–2749. (e) Stone, K. H.; Stephens, P. W.; McConnell, A. C.; Shurdha, E.; Pokhodnya, K. I.; Miller, J. S. $\text{Mn}^{\text{II}}(\text{TCNE})_{3/2}(\text{I}_3)_{1/2}$ —A 3D Network-Structured Organic-Based Magnet and Comparison to a 2D Analog. *Adv. Mater.* **2010**, *22*, 2514–2519. (f) Lapidus, S. H.; McConnell, A. C.; Stephens, P. W.; Miller, J. S. Structure and Magnetic Ordering of a 2-D $\text{Mn}^{\text{II}}(\text{TCNE})\text{I}(\text{OH}_2)$ (TCNE = Tetracyanoethylene) Organic-Based Magnet ($T_c = 171$ K). *Chem. Commun.* **2011**, *47*, 7602–7604. (g) Zhang, J.; Kosaka, W.; Sugimoto, K.; Miyasaka, H. Magnetic Sponge Behavior via Electronic State Modulations. *J. Am. Chem. Soc.* **2018**, *140*, 5644–5652. (5) (a) Mallah, T.; Thiébaut, S.; Verdaguer, M.; Veillet, P. High- T_c Molecular-Based Magnets: Ferrimagnetic Mixed-Valence Chromium(III)-Chromium(II) Cyanides with T_c at 240 and 190 Kelvin. *Science* **1993**, *262*, 1554–1557. (b) Entley, W. R.; Girolami, G. S. High-Temperature Molecular Magnets Based on Cyanovanadate Building Blocks: Spontaneous Magnetization at 230 K. *Science* **1995**, *268*, 397–400. (c) Ferlay, S.; Mallah, T.; Ouahès, R.; Veillet, P.; Verdaguer, M. A Room-Temperature Organometallic Magnet Based on Prussian Blue. *Nature* **1995**, *378*, 701–703. (d) Dujardin, E.; Ferlay, S.; Phan, X.; Desplanches, C.; Cartier dit Moulin, C.; Sainctavit, P.; Baudelet, F.; Dartige, E.; Veillet, P.; Verdaguer, M. Synthesis and Magnetization of New Room-Temperature Molecule-Based Magnets: Effect of Stoichiometry on Local Magnetic Structure by X-ray Magnetic Circular Dichroism. *J. Am. Chem. Soc.* **1998**, *120*, 11347–11352. (6) (a) Larionova, J.; Clérac, R.; Sanchiz, J.; Kahn, O.; Golhen, S.; Ouahab, L. Ferromagnetic Ordering, Anisotropy, and Spin Reorientation for the Cyanide-Bridged Bimetallic Compound $\text{Mn}_2(\text{H}_2\text{O})_5\text{Mo}(\text{CN})_7\cdot 4\text{H}_2\text{O}$ (α Phase). *J. Am. Chem. Soc.* **1998**, *120*, 13088–13095. (b) Holmes, S. M.; Girolami, G. S. Sol–Gel Synthesis of $\text{KV}^{\text{II}}[\text{Cr}^{\text{III}}(\text{CN})_6]\cdot 2\text{H}_2\text{O}$: A Crystalline Molecule-Based Magnet with a Magnetic Ordering Temperature above 100 °C. *J. Am. Chem. Soc.* **1999**, *121*, 5593–5594. (c) Verdaguer, M.; Girolami, G. S. Magnetic Prussian Blue Analogs. In *Magnetism: Molecules to Materials V*; Miller, J. S., Drillon, M., Eds.; Wiley-VCH: Weinheim, Germany, 2005; pp 283–346. (d) Tomono, K.; Tsunobuchi, Y.; Nakabayashi, K.; Ohkoshi, S.-I. Vanadium(II) Heptacyanomolybdate(III)-Based Magnet Exhibiting a High Curie Temperature of 110 K. *Inorg. Chem.* **2010**, *49*, 1298–1300. (e) Her, J.-H.; Stephens, P. W.; Kareis, C. M.; Moore, J. G.; Min, K. S.; Park, J.-W.; Bali, G.; Kennon, B. S.; Miller, J. S. Anomalous Non-Prussian Blue Structures and Magnetic Ordering of $\text{K}_2\text{Mn}^{\text{II}}[\text{Mn}^{\text{II}}(\text{CN})_6]$ and $\text{Rb}_2\text{Mn}^{\text{II}}[\text{Mn}^{\text{II}}(\text{CN})_6]$. *Inorg. Chem.* **2010**, *49*, 1524–1534. (f) Ohkoshi, S.-I.; Imoto, K.; Tsunobuchi, Y.; Takano, S.; Tokoro, H. Light-Induced Spin-Crossover Magnet. *Nat. Chem.* **2011**, *3*, 564–569. (g) Tokoro, H.; Ohkoshi, S.-I. Novel Magnetic Functionalities of Prussian Blue Analogs. *Dalton Trans.* **2011**, *40*, 6825–6833.

- (7) (a) Beauvais, L. G.; Long, J. R. $\text{Co}_3[\text{Co}(\text{CN})_5]_2$: A Microporous Magnet with an Ordering Temperature of 38 K. *J. Am. Chem. Soc.* **2002**, *124*, 12096–12097. (b) Milon, J.; Daniel, M.-C.; Kaiba, A.; Guionneau, P.; Brandès, S.; Sutter, J.-P. Nanoporous Magnets of Chiral and Racemic $[\{\text{Mn}(\text{HL})\}_2\text{Mn}\{\text{Mo}(\text{CN})_7\}_2]$ with Switchable Ordering Temperatures ($T_c = 85 \text{ K} \leftrightarrow 106 \text{ K}$) Driven by H_2O Sorption ($\text{L} = N,N$ -Dimethylalaninol). *J. Am. Chem. Soc.* **2007**, *129*, 13872–13878. (c) Kaye, S. S.; Choi, H. J.; Long, J. R. Generation and O_2 Adsorption Studies of the Microporous Magnets $\text{CsNi}[\text{Cr}(\text{CN})_6]$ ($T_c = 75 \text{ K}$) and $\text{Cr}_3[\text{Cr}(\text{CN})_6]_2 \cdot 6\text{H}_2\text{O}$ ($T_N = 219 \text{ K}$). *J. Am. Chem. Soc.* **2008**, *130*, 16921–16925.
- (8) (a) Maspoch, D.; Ruiz-Molina, D.; Veciana, J. Magnetic Nanoporous Coordination Polymers. *J. Mater. Chem.* **2004**, *14*, 2713–2723. (b) Kurmoo, M. Magnetic Metal–Organic Frameworks. *Chem. Soc. Rev.* **2009**, *38*, 1353–1379. (c) Dechambenoit, P.; Long, J. R. Microporous Magnets. *Chem. Soc. Rev.* **2011**, *40*, 3249–3265. (d) Clemente-León, M.; Coronado, E.; Martí-Gastaldo, C.; Romero, F. M. Multifunctionality in Hybrid Magnetic Materials Based on Bimetallic Oxalate Complexes. *Chem. Soc. Rev.* **2011**, *40*, 473–497. (e) Miller, J. S. Magnetically Ordered Molecule-Based Materials. *Chem. Soc. Rev.* **2011**, *40*, 3266–3296. (f) Coronado, E.; Minguez Espallargas, G. Dynamic Magnetic MOFs. *Chem. Soc. Rev.* **2013**, *42*, 1525–1539. (g) Minguez Espallargas, G.; Coronado, E. Magnetic Functionalities in MOFs: From the Framework to the Pore. *Chem. Soc. Rev.* **2018**, *47*, 533–557.
- (9) (a) Jeon, I.-R.; Negru, B.; Van Duyne, R. P.; Harris, T. D. A 2D Semiquinone Radical-Containing Microporous Magnet with Solvent-Induced Switching from $T_c = 26$ to 80 K. *J. Am. Chem. Soc.* **2015**, *137*, 15699–15702. (b) Darago, L. E.; Aubrey, M. L.; Yu, C. J.; Gonzalez, M. I.; Long, J. R. Electronic Conductivity, Ferrimagnetic Ordering, and Reductive Insertion Mediated by Organic Mixed-Valence in a Ferric Semiquinoid Metal–Organic Framework. *J. Am. Chem. Soc.* **2015**, *137*, 15703–15711. (c) DeGayner, J. A.; Jeon, I.-R.; Sun, L.; Dincă, M.; Harris, T. D. 2D Conductive Iron-Quinoid Magnets Ordering up to $T_c = 105 \text{ K}$ via Heterogenous Redox Chemistry. *J. Am. Chem. Soc.* **2017**, *139*, 4175–4184. (d) Chen, J.; Sekine, Y.; Komatsu, Y.; Hayami, S.; Miyasaka, H. Thermally Induced Valence Tautomeric Transition in a Two-Dimensional Fe-Tetraoxolene Honeycomb Network. *Angew. Chem., Int. Ed.* **2018**, *57*, 12043–12047. (e) Liu, L.; DeGayner, J. A.; Sun, L.; Zee, D. Z.; Harris, T. D. Reversible Redox Switching of Magnetic Order and Electrical Conductivity in a 2D Manganese Benzoquinoid Framework. *Chem. Sci.* **2019**, *10*, 4652–4661.
- (10) (a) Kim, M.; Cahill, J. F.; Su, Y.; Prather, K. A.; Cohen, S. M. Postsynthetic Ligand Exchange as a Route to Functionalization of ‘Inert’ Metal–Organic Frameworks. *Chem. Sci.* **2012**, *3*, 126–130. (b) Brozek, C. K.; Dincă, M. Cation Exchange at the Secondary Building Units of Metal–Organic Frameworks. *Chem. Soc. Rev.* **2014**, *43*, 5456–5467. (c) Evans, J. D.; Sumby, C. J.; Doonan, C. J. Post-Synthetic Metalation of Metal–Organic Frameworks. *Chem. Soc. Rev.* **2014**, *43*, 5933–5951. (d) Deria, P.; Mondloch, J. E.; Karagiari, O.; Bury, W.; Hupp, J. T.; Farha, O. K. Beyond Post-Synthesis Modification: Evolution of Metal–Organic Frameworks via Building Block Replacement. *Chem. Soc. Rev.* **2014**, *43*, 5896–5912. (e) Liu, C.; Luo, T.-Y.; Feura, E. S.; Zhang, C.; Rosi, N. L. Orthogonal Ternary Functionalization of a Mesoporous Metal–Organic Framework via Sequential Postsynthetic Ligand Exchange. *J. Am. Chem. Soc.* **2015**, *137*, 10508–10511. (f) Cohen, S. M. The Postsynthetic Renaissance in Porous Solids. *J. Am. Chem. Soc.* **2017**, *139*, 2855–2863. (g) Bosch, M.; Yuan, S.; Rutledge, W.; Zhou, H.-C. Stepwise Synthesis of Metal–Organic Frameworks. *Acc. Chem. Res.* **2017**, *50*, 857–865. (h) Liu, L.; Li, L.; DeGayner, J. A.; Winegar, P. H.; Fang, Y.; Harris, T. D. Harnessing Structural Dynamics in a 2D Manganese–Benzoquinoid Framework to Dramatically Accelerate Metal Transport in Diffusion-Limited Metal Exchange Reactions. *J. Am. Chem. Soc.* **2018**, *140*, 11444–11453.
- (11) (a) Verdaguer, M.; Bleuzen, A.; Marvaud, V.; Vaissermann, J.; Seuleiman, M.; Desplanches, C.; Scuiller, A.; Train, C.; Garde, R.; Gelly, G.; Lomenech, C.; Rosenman, I.; Veillet, P.; Cartier, C.; Villain, F. Molecules to Build Solids: High T_c Molecule-Based Magnets by Design and Recent Revival of Cyano Complexes Chemistry. *Coord. Chem. Rev.* **1999**, *190*–*192*, 1023–1047. (b) Garde, R.; Villain, F.; Verdaguer, M. Molecule-Based Room-Temperature Magnets: Catalytic Role of V(III) in the Synthesis of Vanadium–Chromium Prussian Blue Analogues. *J. Am. Chem. Soc.* **2002**, *124*, 10531–10538. (c) Podgajny, R.; Pinkowicz, D.; Korzeniak, T.; Nitek, W.; Rams, M.; Sieklucka, B. High T_c Ferrimagnetic Organic–Inorganic Hybrid Materials with $\text{Mn}^{\text{II}}\text{—L—Mn}^{\text{II}}$ and $\text{Mn}^{\text{II}}\text{—NC—Nb}^{\text{IV}}$ Linkages ($\text{L} = \text{Pyrazine, Pyrazine-N,N'-dioxide, Bipyrimidine}$). *Inorg. Chem.* **2007**, *46*, 10416–10425. (d) Toma, L. M.; Ruiz-Pérez, C.; Pasán, J.; Wernsdorfer, W.; Lloret, F.; Julve, M. Molecular Engineering to Control the Magnetic Interaction Between Single-Chain Magnets Assembled in a Two-Dimensional Network. *J. Am. Chem. Soc.* **2012**, *134*, 15265–15268.
- (12) (a) Wang, X.-Y.; Wang, Z.-M.; Gao, S. Constructing Magnetic Molecular Solids by Employing Three-Atom Ligands as Bridges. *Chem. Commun.* **2008**, 281–294. (b) Pardo, E.; Ruiz-García, R.; Cano, J.; Ottenwaelder, X.; Lescouëzec, R.; Journaux, Y.; Lloret, F.; Julve, M. Ligand Design for Multidimensional Magnetic Materials: A Metallocsupramolecular Perspective. *Dalton Trans.* **2008**, 2780–2805.
- (13) (a) Caneschi, A.; Gatteschi, D.; Sessoli, R.; Rey, P. Toward Molecular Magnets: The Metal–Radical Approach. *Acc. Chem. Res.* **1989**, *22*, 392–398. (b) Faust, T. B.; D’Alessandro, D. M. Radicals in Metal–Organic Frameworks. *RSC Adv.* **2014**, *4*, 17498–17512.
- (14) (a) Miyasaka, H.; Izawa, T.; Takahashi, N.; Yamashita, M.; Dunbar, K. R. Long-Range Ordered Magnet of a Charge-Transfer $\text{Ru}_2^{4+}/\text{TCNQ}$ Two-Dimensional Network Compound. *J. Am. Chem. Soc.* **2006**, *128*, 11358–11359. (b) Motokawa, N.; Miyasaka, H.; Yamashita, M.; Dunbar, K. R. An Electron-Transfer Ferromagnet with $T_c = 107 \text{ K}$ Based on a Three-Dimensional $[\text{Ru}_2]_2/\text{TCNQ}$ System. *Angew. Chem., Int. Ed.* **2008**, *47*, 7760–7763. (c) Miyasaka, H.; Motokawa, N.; Matsunaga, S.; Yamashita, M.; Sugimoto, K.; Mori, T.; Toyota, N.; Dunbar, K. R. Control of Charge Transfer in a Series of $\text{Ru}_2^{\text{II,II}}/\text{TCNQ}$ Two-Dimensional Networks by Tuning the Electron Affinity of TCNQ Units: A Route to Synergistic Magnetic/Conducting Materials. *J. Am. Chem. Soc.* **2010**, *132*, 1532–1544. (d) Kobayashi, Y.; Jacobs, B.; Allendorf, M. D.; Long, J. R. Conductivity, Doping, and Redox Chemistry of a Microporous Dithiolene-Based Metal–Organic Framework. *Chem. Mater.* **2010**, *22*, 4120–4122. (e) Talin, A. A.; Centrone, A.; Ford, A. C.; Foster, M. E.; Stavila, V.; Haney, P.; Kinney, R. A.; Szalai, V.; El Gabaly, F.; Yoon, H. P.; Léonard, F.; Allendorf, M. D. Tunable Electrical Conductivity in Metal–Organic Framework Thin-Film Devices. *Science* **2014**, *343*, 66–69. (f) Nidamanuri, N.; Saha, S. Metal–Organic Frameworks with Tunable Electrical and Optical Properties. In *Monographs in Supramolecular Chemistry*; Banerjee, R., Ed.; The Royal Society of Chemistry: Cambridge, UK, 2017; Vol. 22, pp 217–246.
- (g) Benmansour, S.; Abhervé, A.; Gómez-Claramunt, P.; Vallés-García, C.; Gómez-García, C. J. Nanosheets of Two-Dimensional Magnetic and Conducting $\text{Fe}(\text{II})/\text{Fe}(\text{III})$ Mixed-Valence Metal–Organic Frameworks. *ACS Appl. Mater. Interfaces* **2017**, *9*, 26210–26218. (h) Yang, C.; Dong, R.; Wang, M.; Petkov, P. S.; Zhang, Z.; Wang, M.; Han, P.; Ballabio, M.; Bräuningher, S. A.; Liao, Z.; Zhang, J.; Schwotzer, F.; Zschech, E.; Klauss, H.-H.; Cánovas, E.; Kaskel, S.; Bonn, M.; Zhou, S.; Heine, T.; Feng, X. A Semiconducting Layered Metal–Organic Framework Magnet. *Nat. Commun.* **2019**, *10*, 3260.
- (15) (a) Chelebaeva, E.; Larionova, J.; Guari, Y.; Ferreira, R. A. S.; Carlos, L. D.; Almeida Paz, F. A.; Trifonov, A.; Guérin, C. Luminescent and Magnetic Cyano-Bridged Coordination Polymers Containing 4d–4f Ions: Toward Multifunctional Materials. *Inorg. Chem.* **2009**, *48*, 5983–5995. (b) Ferrando-Soria, J.; Khajavi, H.; Serra-Crespo, P.; Gascon, J.; Kapteijn, F.; Julve, M.; Lloret, F.; Pasán, J.; Ruiz-Pérez, C.; Journaux, Y.; Pardo, E. Highly Selective Chemical Sensing in a Luminescent Nanoporous Magnet. *Adv. Mater.* **2012**, *24*, 5625–5629. (c) Chelebaeva, E.; Long, J.; Larionova, J.; Ferreira, R. A. S.; Carlos, L. D.; Almeida Paz, F. A.; Gomes, J. B. R.; Trifonov, A.; Guérin, C.; Guari, Y. Bifunctional Mixed-Lanthanide Cyano-Bridged Coordination Polymers $\text{Ln}_{0.5}\text{Ln}'_{0.5}(\text{H}_2\text{O})_5[\text{W}(\text{CN})_8]$ ($\text{Ln/Ln}' =$

- $\text{Eu}^{3+}/\text{Tb}^{3+}$, $\text{Eu}^{3+}/\text{Gd}^{3+}$, $\text{Tb}^{3+}/\text{Sm}^{3+}$). *Inorg. Chem.* **2012**, *51*, 9005–9016. (d) Chorazy, S.; Nakabayashi, K.; Ohkoshi, S.-I.; Sieklucka, B. Green to Red Luminescence Switchable by Excitation Light in Cyanido-Bridged $\text{Tb}^{\text{III}}-\text{W}^{\text{V}}$ Ferromagnet. *Chem. Mater.* **2014**, *26*, 4072–4075. (e) van der Meer, M.; Rechkemmer, Y.; Breitgoff, F. D.; Marx, R.; Neugebauer, P.; Frank, U.; van Slageren, J.; Sarkar, B. Multiple Bistability in Quinonoid-Bridged Diiron(II) Complexes: Influence of Bridge Symmetry on Bistable Properties. *Inorg. Chem.* **2016**, *55*, 11944–11953. (f) Perfetti, M.; Pointillart, F.; Cador, O.; Sorace, L.; Ouahab, L. Luminescent Molecular Magnets. In *Molecular Magnetic Materials: Concepts and Applications*; Sieklucka, B., Pinkowicz, D., Eds.; Wiley-VCH: Weinheim, Germany, 2017; pp 345–368. (g) Benmansour, S.; Cerezo-Navarrete, C.; Canet-Ferrer, J.; Muñoz-Matutano, G.; Martínez-Pastor, J.; Gómez-García, C. J. A Fluorescent Layered Oxalato-Based Canted Antiferromagnet. *Dalton Trans.* **2018**, *47*, 11909–11916.
- (16) (a) Rocha, A. R.; García-Suárez, V. M.; Bailey, S. W.; Lambert, C. J.; Ferrer, J.; Sanvito, S. Towards Molecular Spintronics. *Nat. Mater.* **2005**, *4*, 335–339. (b) Bogani, L.; Wernsdorfer, W. Molecular Spintronics Using Single-Molecule Magnets. *Nat. Mater.* **2008**, *7*, 179–186. (c) Ardavan, A.; Blundell, S. J. Storing Quantum Information in Chemically Engineered Nanoscale Magnets. *J. Mater. Chem.* **2009**, *19*, 1754–1760. (d) Liu, H.; Zhang, C.; Malissa, H.; Groesbeck, M.; Kavand, M.; McLaughlin, R.; Jamali, S.; Hao, J.; Sun, D.; Davidson, R. A.; Wojcik, L.; Miller, J. S.; Boehme, C.; Vardeny, Z. V. Organic-Based Magnon Spintronics. *Nat. Mater.* **2018**, *17*, 308–312.
- (17) (a) Gwak, J.; Ayral, A.; Rouessac, V.; Cot, L.; Grenier, J.-C.; Choy, J.-H. Synthesis and Characterization of Porous Ferrimagnetic Membranes. *Microporous Mesoporous Mater.* **2003**, *63*, 177–184. (b) Madaeni, S. S.; Enayati, E.; Vatanpour, V. Separation of Nitrogen and Oxygen Gases by Polymeric Membrane Embedded with Magnetic Nano-Particle. *Polym. Adv. Technol.* **2011**, *22*, 2556–2563. (c) Ferrando-Soria, J.; Serra-Crespo, P.; de Lange, M.; Gascon, J.; Kapteijn, F.; Julve, M.; Cano, J.; Lloret, F.; Pasán, J.; Ruiz-Pérez, C.; Journaux, Y.; Pardo, E. Selective Gas and Vapor Sorption and Magnetic Sensing by an Isoreticular Mixed-Metal–Organic Framework. *J. Am. Chem. Soc.* **2012**, *134*, 15301–15304.
- (18) Krishnan, K. M. *Fundamentals and Applications of Magnetic Materials*; Oxford University Press: Oxford, UK, 2016.
- (19) Kahn, O. *Molecular Magnetism*; VCH: New York, 1993.
- (20) (a) Coulon, C.; Miyasaka, H.; Clérac, R. Single-Chain Magnets: Theoretical Approach and Experimental Systems. In *Single-Molecule Magnets and Related Phenomena. Structure and Bonding*; Winpenny, R. E. P., Ed.; Springer-Verlag: Berlin, Germany, 2006; Vol. 122, pp 163–206. (b) Gatteschi, D.; Vindigni, A. Single-Chain Magnets. In *Molecular Magnets: Physics and Applications*; Bartolomé, J., Luis, F., Fernández, J. F., Eds.; Springer-Verlag: Berlin, Germany, 2014; Vol. 1, pp 191–220. (c) Coulon, C.; Pianet, V.; Urdampilleta, M.; Clérac, R. Single-Chain Magnets and Related Systems. In *Molecular Nanomagnets and Related Phenomena. Structure and Bonding*; Gao, S., Ed.; Springer-Verlag: Berlin, Germany, 2014; Vol. 164, pp 143–184.
- (21) Domb, C. Ising Model. In *Phase Transitions and Critical Phenomena*; Domb, C., Green, M. S., Eds.; Academic Press: London, UK, 1974; Vol. 3, pp 357–484.
- (22) (a) Vostrikova, K. E. High-Spin Molecules Based on Metal Complexes of Organic Free Radicals. *Coord. Chem. Rev.* **2008**, *252*, 1409–1419. (b) *Stable Radicals: Fundamentals and Applied Aspects of Odd Electron Compounds*; Hicks, R. G., Ed.; John Wiley & Sons, Inc.: Chichester, UK, 2010. (c) Lemaire, M. T. Progress and Design Challenges for High-Spin Molecules. *Pure Appl. Chem.* **2010**, *83*, 141–149. (d) Iwamura, H. What Role Has Organic Chemistry Played in the Development of Molecule-Based Magnets? *Polyhedron* **2013**, *66*, 3–14.
- (23) Selected references: (a) Caneschi, A.; Gatteschi, D.; Laugier, J.; Rey, P. Ferromagnetic Alternating Spin Chains. *J. Am. Chem. Soc.* **1987**, *109*, 2191–2192. (b) Caneschi, A.; Gatteschi, D.; Renard, J. P.; Rey, P.; Sessoli, R. Magnetic Phase Transitions in Manganese(II) Pentafluorobenzoate Adducts with Nitronyl Nitroxides. *J. Am. Chem. Soc.* **1989**, *111*, 785–786. (c) Caneschi, A.; Ferraro, F.; Gatteschi, D.; Rey, P.; Sessoli, R. Structure and Magnetic Properties of a Chain Compound Formed by Copper(II) and a Tridentate Nitronyl Nitroxide Radical. *Inorg. Chem.* **1991**, *30*, 3162–3166. (d) Caneschi, A.; Gatteschi, D.; Rey, P.; Sessoli, R. Structure and Magnetic Ordering of a Ferrimagnetic Helix Formed by Manganese(II) and a Nitronyl Nitroxide Radical. *Inorg. Chem.* **1991**, *30*, 3936–3941. (e) Stumpf, H. O.; Ouahab, L.; Pei, Y.; Grandjean, D.; Kahn, O. A Molecular-Based Magnet with a Fully Interlocked Three-Dimensional Structure. *Science* **1993**, *261*, 447–449. (f) Inoue, K.; Iwamura, H. Ferro- and Ferrimagnetic Ordering in a Two-Dimensional Network Formed by Manganese(II) and 1,3,5-Tris[*p*-(*N*-tert-butyl-*N*-oxamino)phenyl]-benzene. *J. Am. Chem. Soc.* **1994**, *116*, 3173–3174. (g) Caneschi, A.; Gatteschi, D.; Le Lirzin, A. Crystal Structure and Magnetic Properties of a New Ferrimagnetic Chain Containing Manganese(II) and a Nitronyl-Nitroxide Radical. Magnetic Ordering in $\text{Mn}(\text{hfac})_2\text{NITR}$ Compounds. *J. Mater. Chem.* **1994**, *4*, 319–326. (h) Inoue, K.; Hayamizu, T.; Iwamura, H.; Hashizume, D.; Ohashi, Y. Assemblage and Alignment of the Spins of the Organic Trinitroxide Radical with a Quartet Ground State by Means of Complexation with Magnetic Metal Ions. A Molecule-Based Magnet with Three-Dimensional Structure and High T_C of 46 K. *J. Am. Chem. Soc.* **1996**, *118*, 1803–1804. (i) Fegy, K.; Luneau, D.; Ohm, T.; Paulsen, C.; Rey, P. Two-Dimensional Nitroxide-Based Molecular Magnetic Materials. *Angew. Chem., Int. Ed.* **1998**, *37*, 1270–1273. (j) Numata, Y.; Inoue, K.; Baranov, N.; Kurmoo, M.; Kikuchi, K. Field-Induced Ferrimagnetic State in a Molecule-Based Magnet Consisting of a Co^{II} Ion and a Chiral Triplet Bis(nitroxide) Radical. *J. Am. Chem. Soc.* **2007**, *129*, 9902–9909. (k) Meng, X.; Shi, W.; Cheng, P. Magnetism in One-Dimensional Metal–Nitronyl Nitroxide Radical System. *Coord. Chem. Rev.* **2019**, *378*, 134–150. (l) Liu, X.; Wang, Y.-X.; Han, Z.; Han, T.; Shi, W.; Cheng, P. Tuning the Magnetization Dynamics of Tb^{III} -Based Single-Chain Magnets Through Substitution on the Nitronyl Nitroxide Radical. *Dalton Trans.* **2019**, *48*, 8989–8994.
- (24) Selected references: (a) Du, G.; Joo, J.; Epstein, A. J.; Miller, J. S. Anomalous Charge Transport Phenomena in Molecular-Based Magnet $\text{V}(\text{TCNE})_{x,y}(\text{solvent})$. *J. Appl. Phys.* **1993**, *73*, 6566–6568. (b) Zhao, H.; Heintz, R. A.; Ouyang, X.; Dunbar, K. R.; Campana, C. F.; Rogers, R. D. Spectroscopic, Thermal, and Magnetic Properties of Metal/TCNQ Network Polymers with Extensive Supramolecular Interactions Between Layers. *Chem. Mater.* **1999**, *11*, 736–746. (c) Clérac, R.; O’Kane, S.; Cowen, J.; Ouyang, X.; Heintz, R.; Zhao, H.; Bazile, M. J., Jr.; Dunbar, K. R. Glassy Magnets Composed of Metals Coordinated to 7,7,8,8-Tetracyanoquinodimethane: $\text{M}-(\text{TCNQ})_2$ ($\text{M} = \text{Mn, Fe, Co, Ni}$). *Chem. Mater.* **2003**, *15*, 1840–1850. (d) Motokawa, N.; Matsunaga, S.; Takaishi, S.; Miyasaka, H.; Yamashita, M.; Dunbar, K. R. Reversible Magnetism Between an Antiferromagnet and a Ferromagnet Related to Solvation/Desolvation in a Robust Layered $[\text{Ru}_{12}]_2\text{TCNQ}$ Charge-Transfer System. *J. Am. Chem. Soc.* **2010**, *132*, 11943–11951. (e) McConnell, A. C.; Fishman, R. S.; Miller, J. S. Mean Field Analysis of the Exchange Coupling (J) for Two-and Three-Dimensional Structured Tetracyanoethenide (TCNE[–])-Based Magnets. *J. Phys. Chem. C* **2012**, *116*, 16154–16160. (f) Pokhodnya, K.; Bonner, M.; Prigodin, V.; Epstein, A. J.; Miller, J. S. Carrier Transport in the $\text{V}[\text{TCNE}]_x$ ($\text{TCNE} = \text{Tetracyanoethylene}$; $x \sim 2$) Organic-Based Magnet. *J. Phys.: Condens. Matter* **2013**, *25*, 196001. (g) Olson, C. S.; Gangopadhyay, S.; Hoang, K.; Alema, F.; Kilina, S.; Pokhodnya, K. Magnetic Exchange in $\text{Mn}^{\text{II}}[\text{TCNE}]$ ($\text{TCNE} = \text{Tetracyanoethylene}$) Molecule-Based Magnets with Two- and Three-Dimensional Magnetic Networks. *J. Phys. Chem. C* **2015**, *119*, 25036–25046.
- (25) (a) Maspoch, D.; Ruiz-Molina, D.; Wurst, K.; Domingo, N.; Cavallini, M.; Biscarini, F.; Tejada, J.; Rovira, C.; Veciana, J. A Nanoporous Molecular Magnet with Reversible Solvent-Induced Mechanical and Magnetic Properties. *Nat. Mater.* **2003**, *2*, 190–195. (b) Maspoch, D.; Domingo, N.; Ruiz-Molina, D.; Wurst, K.; Hernández, J.-M.; Vaughan, G.; Rovira, C.; Lloret, F.; Tejada, J.; Veciana, J. Coexistence of Ferro- and Antiferromagnetic Interactions

- in a Metal–Organic Radical-Based (6,3)-Helical Network with Large Channels. *Chem. Commun.* **2005**, 5035–5037.
- (26) (a) Koga, N.; Ishimaru, Y.; Iwamura, H. Diazodi(4-pyridyl)methane and Diazophenyl-(4-pyridyl)methane as Photoresponsive Ligands for Metal–Carbene Hetero-Spin Systems. *Angew. Chem., Int. Ed. Engl.* **1996**, *35*, 755–757. (b) Yoshihara, D.; Karasawa, S.; Koga, N. Cyclic Single-Molecule Magnet in Heterospin System. *J. Am. Chem. Soc.* **2008**, *130*, 10460–10461. (c) Yoshihara, D.; Karasawa, S.; Koga, N. Heterospin Single-Molecule Magnets with Extra-Large Anisotropic Barrier. *Polyhedron* **2011**, *30*, 3211–3217.
- (27) Pedersen, K. S.; Perlepe, P.; Aubrey, M. L.; Woodruff, D. N.; Reyes-Lillo, S. E.; Reinholdt, A.; Voigt, L.; Li, Z.; Borup, K.; Rouzières, M.; Samohvalov, D.; Wilhelm, F.; Rogalev, A.; Neaton, J. B.; Long, J. R.; Clérac, R. Formation of the Layered Conductive Magnet $\text{CrCl}_2(\text{pyrazine})_2$ Through Redox-Active Coordination Chemistry. *Nat. Chem.* **2018**, *10*, 1056–1061.
- (28) (a) Johnston, R. F.; Holwerda, R. A. Ethanol Oxidation by Chromium(III) Complexes of Chloranilic Acid. Spectroscopic, Electrochemical, Magnetic, and Chromatographic Studies of Chloranilate Semiquinone-Bridged Polynuclear Chromium Ions. *Inorg. Chem.* **1985**, *24*, 153–159. (b) Dei, A.; Gatteschi, D.; Pardi, L.; Russo, U. Tetraoxolene Radical Stabilization by the Interaction with Transition-Metal Ions. *Inorg. Chem.* **1991**, *30*, 2589–2594. (c) Min, K. S.; Rheingold, A. L.; DiPasquale, A. G.; Miller, J. S. Characterization of the Chloranilate(-3-) π Radical as a Strong Spin-Coupling Bridging Ligand. *Inorg. Chem.* **2006**, *45*, 6135–6137. (d) Min, K. S.; DiPasquale, A. G.; Golen, J. A.; Rheingold, A. L.; Miller, J. S. Synthesis, Structure, and Magnetic Properties of Valence Ambiguous Dinuclear Antiferromagnetically Coupled Cobalt and Ferromagnetically Coupled Iron Complexes Containing the Chloranilate(2-) and the Significantly Stronger Coupling Chloranilate(-3-) Radical Trianion. *J. Am. Chem. Soc.* **2007**, *129*, 2360–2368. (e) Guo, D.; McCusker, J. K. Spin Exchange Effects on the Physicochemical Properties of Tetraoxolene-Bridged Bimetallic Complexes. *Inorg. Chem.* **2007**, *46*, 3257–3274. (f) Miller, J. S.; Min, K. S. Oxidation Leading to Reduction: Redox-Induced Electron Transfer (RIET). *Angew. Chem., Int. Ed.* **2009**, *48*, 262–272. (g) Baum, A. E.; Lindeman, S. V.; Fiedler, A. T. Preparation of a Semiquinonate-Bridged Diiron(II) Complex and Elucidation of Its Geometric and Electronic Structures. *Chem. Commun.* **2013**, *49*, 6531–6533.
- (29) (a) Jeon, I.-R.; Park, J. G.; Xiao, D. J.; Harris, T. D. An Azophenine Radical-Bridged Fe_2 Single-Molecule Magnet with Record Magnetic Exchange Coupling. *J. Am. Chem. Soc.* **2013**, *135*, 16845–16848. (b) DeGayner, J. A.; Jeon, I.-R.; Harris, T. D. A Series of Tetraazalene Radical-Bridged M_2 ($M = \text{Cr}^{\text{III}}$, Mn^{II} , Fe^{II} , Co^{II}) Complexes with Strong Magnetic Exchange Coupling. *Chem. Sci.* **2015**, *6*, 6639–6648. (c) Hua, C.; DeGayner, J. A.; Harris, T. D. Thiosemiquinoid Radical-Bridged Cr^{III}_2 Complexes with Strong Magnetic Exchange Coupling. *Inorg. Chem.* **2019**, *58*, 7044–7053.
- (30) Jeon, I.-R.; Sun, L.; Negru, B.; Van Duyne, R. P.; Dincă, M.; Harris, T. D. Solid-State Redox Switching of Magnetic Exchange and Electronic Conductivity in a Benzoquinonoid-Bridged Mn^{II} Chain Compound. *J. Am. Chem. Soc.* **2016**, *138*, 6583–6590.
- (31) Murase, R.; Abrahams, B. F.; D’Alessandro, D. M.; Davies, C. G.; Hudson, T. A.; Jameson, G. N. L.; Moubaraki, B.; Murray, K. S.; Robson, R.; Sutton, A. L. Mixed Valency in a 3D Semiconducting Iron–Fluoranyl Coordination Polymer. *Inorg. Chem.* **2017**, *56*, 9025–9035.
- (32) (a) Tinti, F.; Verdaguier, M.; Kahn, O.; Savariault, J.-M. Interaction Between Copper(II) Ions Separated by 7.6 Å. Crystal Structure and Magnetic Properties of (μ -Iodanilate)bis[(*N,N,N’,N’*-tetramethylethylenediamine)copper(II)] Diperchlorate. *Inorg. Chem.* **1987**, *26*, 2380–2384. (b) Schweinfurth, D.; Khusniyarov, M. M.; Bubrin, D.; Hohloch, S.; Su, C.-Y.; Sarkar, B. Tuning Spin–Spin Coupling in Quinonoid-Bridged Dicopper(II) Complexes Through Rational Bridge Variation. *Inorg. Chem.* **2013**, *52*, 10332–10339.
- (33) Atzori, M.; Benmansour, S.; Minguez Espallargas, G.; Clemente-León, M.; Abhervé, A.; Gómez-Claramunt, P.; Coronado, E.; Artizzi, F.; Sessini, E.; Deplano, P.; Serpe, A.; Mercuri, M. L.; Gómez-García, C. J. A Family of Layered Chiral Porous Magnets Exhibiting Tunable Ordering Temperatures. *Inorg. Chem.* **2013**, *52*, 10031–10040.
- (34) (a) Sloop, J. C. Substituent Effects on Spin Density Distribution and Exchange Coupling in Semiquinone Complexes. Ph.D. Dissertation, North Carolina State University: Raleigh, NC, 2003. (b) Shultz, D. A.; Sloop, J. C.; Coote, T.-A.; Beikmohammadi, M.; Kampf, J.; Boyle, P. D. Substituent Effects on Exchange Coupling: S-Aryl-Substituted Semiquinones and Their Complexes with Mn^{II} and Cu^{II} . *Inorg. Chem.* **2007**, *46*, 273–277.
- (35) Baum, A. E.; Park, H.; Wang, D.; Lindeman, S. V.; Fiedler, A. T. Structural, Spectroscopic, and Electrochemical Properties of Non-heme $\text{Fe}(\text{II})$ –Hydroquinonate Complexes: Synthetic Models of Hydroquinone Dioxygenases. *Dalton Trans.* **2012**, *41*, 12244–12253.
- (36) Park, J. G.; Jeon, I.-R.; Harris, T. D. Electronic Effects of Ligand Substitution on Spin Crossover in a Series of Diiminoquinonoid-Bridged Fe^{II}_2 Complexes. *Inorg. Chem.* **2015**, *54*, 359–369.
- (37) Min, K. S.; Swierczek, K.; DiPasquale, A. G.; Rheingold, A. L.; Reiff, W. M.; Arif, A. M.; Miller, J. S. A Dinuclear Iron(II) Complex, [(TPyA) $\text{Fe}^{\text{II}}(\text{THBQ}^{2-})\text{Fe}^{\text{II}}(\text{TPyA})$](BF_4)₂ [TPyA = Tris(2-pyridylmethyl)amine; THBQ²⁻ = 2,3,5,6-Tetrahydroxy-1,4-benzoquinonate] Exhibiting both Spin Crossover with Hysteresis and Ferromagnetic Exchange. *Chem. Commun.* **2008**, 317–319.
- (38) Feilchenfeld, H. A Relation Between the Lengths of Single, Double and Triple Bonds. *J. Phys. Chem.* **1959**, *63*, 1346.
- (39) Drew, M. G. B.; Harding, C. J.; McKee, V.; Morgan, G. G.; Nelson, J. Geometric Control of Manganese Redox State. *J. Chem. Soc., Chem. Commun.* **1995**, 1035–1038.
- (40) Gaudette, A. I.; Jeon, I.-R.; Anderson, J. S.; Grandjean, F.; Long, G. J.; Harris, T. D. Electron Hopping Through Double-Exchange Coupling in a Mixed-Valence Diiminobenzoquinone-Bridged Fe_2 Complex. *J. Am. Chem. Soc.* **2015**, *137*, 12617–12626.
- (41) Hansch, C.; Leo, A.; Taft, R. W. A Survey of Hammett Substituent Constants and Resonance and Field Parameters. *Chem. Rev.* **1991**, *91*, 165–195.
- (42) Li, F.; Chakrabarti, M.; Dong, Y.; Kauffmann, K.; Bominaar, E. L.; Münck, E.; Que, L., Jr. Structural, EPR, and Mössbauer Characterization of (μ -Alkoxo)(μ -Carboxylato)Diiron(II,III) Model Complexes for the Active Sites of Mixed-Valent Diiron Enzymes. *Inorg. Chem.* **2012**, *51*, 2917–2929.
- (43) (a) Kawata, S.; Kitagawa, S.; Kumagai, H.; Ishiyama, T.; Honda, K.; Tobita, H.; Adachi, K.; Katada, M. Novel Intercalation Host System Based on Transition Metal (Fe^{2+} , Co^{2+} , Mn^{2+})–Chloranilate Coordination Polymers. Single Crystal Structures and Properties. *Chem. Mater.* **1998**, *10*, 3902–3912. (b) Nagayoshi, K.; Kabir, M. K.; Tobita, H.; Honda, K.; Kawahara, M.; Katada, M.; Adachi, K.; Nishikawa, H.; Ikemoto, I.; Kumagai, H.; Hosokoshi, Y.; Inoue, K.; Kitagawa, S.; Kawata, S. Design of Novel Inorganic–Organic Hybrid Materials Based on Iron-Chloranilate Mononuclear Complexes: Characteristics of Hydrogen-Bond-Supported Layers Toward the Intercalation of Guests. *J. Am. Chem. Soc.* **2003**, *125*, 221–232.
- (44) (a) Kessel, S. L.; Hendrickson, D. N. Magnetic Exchange Interactions in Binuclear Transition-Metal Complexes. 16. Binuclear Ferric Complexes from the Reaction of $\text{Fe}^{\text{II}}(\text{salen})$ with *p*-Quinones. *Inorg. Chem.* **1978**, *17*, 2630–2636. (b) Iijima, S.; Mizutani, F.; Mitsumi, M.; Matsumoto, N.; Okawa, H. Slow Paramagnetic Relaxation and Magnetic Splittings in Mössbauer Spectra Observed for Mixed-Metal Assemblies $\{\text{NBu}_4\text{MFe}(\text{ox})_3\}_x$ (NBu_4^+ = Tetra(n-butyl)ammonium Ion; ox^{2-} = Oxalate Ion; $M = \text{Zn}^{2+}$, Ni^{2+} , Mn^{2+}). *Inorg. Chim. Acta* **1996**, *253*, 47–51. (c) Scepaniak, J. J.; Vogel, C. S.; Khusniyarov, M. M.; Heinemann, F. W.; Meyer, K.; Smith, J. M. Synthesis, Structure, and Reactivity of an Iron(V) Nitride. *Science* **2011**, *331*, 1049–1052. (d) Zadrozy, J. M.; Xiao, D. J.; Long, J. R.; Atanasov, M.; Neese, F.; Grandjean, F.; Long, G. J. Mössbauer Spectroscopy as a Probe of Magnetization Dynamics in the Linear Iron(I) and Iron(II) Complexes $[\text{Fe}(\text{C}(\text{SiMe}_3)_3)_2]^{1/0}$. *Inorg. Chem.* **2013**, *52*, 13123–13131. (e) Valdez-Moreira, J. A.; Thorarinsdottir, A. E.; DeGayner, J. A.; Lutz, S. A.; Chen, C.-H.; Losovy, Y.; Pink, M.;

- Harris, T. D.; Smith, J. M. Strong π -Backbonding Enables Record Magnetic Exchange Coupling Through Cyanide. *J. Am. Chem. Soc.* **2019**, *141*, 17092–17097.
- (45) (a) Pfannes, H.-D.; Gonser, U. Goldanskii-Karyagin Effect Versus Preferred Orientations (Texture). *Appl. Phys.* **1973**, *1*, 93–102. (b) Ellwood, B. B.; Burkart, B.; Rajeshwar, K.; Darwin, R. L.; Neeley, R. A.; McCall, A. B.; Long, G. J.; Buhl, M. L.; Hickcox, C. W. Are the Iron Carbonate Minerals, Ankerite and Ferroan Dolomite, Like Siderite, Important in Paleomagnetism? *J. Geophys. Res.* **1989**, *94*, 7321–7331.
- (46) Weisser, F.; Stevens, H.; Klein, J.; van der Meer, M.; Hohloch, S.; Sarkar, B. Tailoring Ru^{II} Pyridine/Triazole Oxygenation Catalysts and Using Photoreactivity to Probe Their Electronic Properties. *Chem. - Eur. J.* **2015**, *21*, 8926–8938.
- (47) (a) Mulyana, Y.; Alley, K. G.; Davies, K. M.; Abrahams, B. F.; Moubaraki, B.; Murray, K. S.; Boskovic, C. Dinuclear Cobalt(II) and Cobalt(III) Complexes of Bis-Bidentate Naphthoquinone Ligands. *Dalton Trans.* **2014**, *43*, 2499–2511. (b) Atzori, M.; Artizzu, F.; Marchio, L.; Loche, D.; Caneschi, A.; Serpe, A.; Deplano, P.; Avarvari, N.; Mercuri, M. L. Switching-On Luminescence in Anilate-Based Molecular Materials. *Dalton Trans.* **2015**, *44*, 15786–15802.
- (48) (a) Lukov, V. V.; Levchenkov, S. I.; Shcherbakov, I. N.; Posokhova, S. V.; Kogan, V. A. Structure and Magnetic Characteristics of New Binuclear Complexes Based on Bisbenzoylhydrazones of 2,6-Diformyl-4-R-phenols and Copper(II) Nitrate. *Russ. J. Coord. Chem.* **2001**, *27*, 135–137. (b) Prat, I.; Company, A.; Corona, T.; Parella, T.; Ribas, X.; Costas, M. Assessing the Impact of Electronic and Steric Tuning of the Ligand in the Spin State and Catalytic Oxidative Ability of the Fe^{II}(Pytacn) Family of Complexes. *Inorg. Chem.* **2013**, *52*, 9229–9244.
- (49) Starikov, A. G.; Chegerek, M. G.; Starikova, A. A.; Minkin, V. I. Magnetic Properties of the Dicationic Iron *o*-Quinone Complexes with the Pyridinophane Ligands: A Quantum Chemical Study. *Russ. J. Coord. Chem.* **2019**, *45*, 675–679.
- (50) Starikova, A. A.; Starikov, A. G.; Minkin, V. I. Dinuclear Adducts of Di-*o*-Iminoquinone Ligands with Co^{II} Diketonates: Computational Insights into Two-Step Valence Tautomeric Rearrangements. *J. Mol. Model.* **2017**, *23*, 307.
- (51) (a) Chlopek, K.; Bothe, E.; Neese, F.; Weyhermüller, T.; Wieghardt, K. Molecular and Electronic Structures of Tetrahedral Complexes of Nickel and Cobalt Containing *N,N'*-Disubstituted, Bulky *o*-Diiminobenzosemiquinonate(1-) π -Radical Ligands. *Inorg. Chem.* **2006**, *45*, 6298–6307. (b) Ali, A.; Dhar, D.; Barman, S. K.; Lloret, F.; Mukherjee, R. Nickel(II) Complex of a Hexadentate Ligand with Two *o*-Iminosemiquinonato(1-) π -Radical Units and Its Monocation and Dication. *Inorg. Chem.* **2016**, *55*, 5759–5771. (c) Sheepwash, M. A. L.; Lough, A. J.; Poggini, L.; Poneti, G.; Lemaire, M. T. Structure, Magnetic Properties and Electronic Structure of a Nickel(II) Complex with Redox-Active 6-(8-Quinolylamino)-2,4-bis-(*tert*-butyl)phenol. *Polyhedron* **2016**, *108*, 2–7.
- (52) Kundu, T.; Sarkar, B.; Mondal, T. K.; Mobin, S. M.; Urbanos, F. A.; Fiedler, J.; Jiménez-Aparicio, R.; Kaim, W.; Lahiri, G. K. Redox-Rich Spin-Spin-Coupled Semiquinoneruthenium Dimers with Intense Near-IR Absorption. *Inorg. Chem.* **2011**, *50*, 4753–4763.
- (53) Deibel, N.; Hohloch, S.; Schweinfurth, D.; Weisser, F.; Grupp, A.; Sarkar, B. Three-Way Cooperativity in d⁸ Metal Complexes with Ligands Displaying Chemical and Redox Non-Innocence. *Chem. - Eur. J.* **2014**, *20*, 15178–15187.
- (54) One counterexample is a semiquinoid-bridged Ga^{III}₂ complex that has been reported to exhibit unpaired spin density but no electron density on Cl substituents and associated C atoms of the ring; see Schrauben, J. N.; Guo, D.; McCracken, J. L.; McCusker, J. K. Electronic Structure of [Ga₂(tren)₂(CA^{sq,cat})](BPh₄)₂(BF₄): An EPR, ENDOR, and Density Functional Study. *Inorg. Chim. Acta* **2008**, *361*, 3539–3547.
- (55) (a) Cole, K. S.; Cole, R. H. Dispersion and Absorption in Dielectrics I. Alternating Current Characteristics. *J. Chem. Phys.* **1941**, *9*, 341–351. (b) Böttcher, C. J. F. *Theory of Electric Polarisation*; Elsevier: Amsterdam, Netherlands, 1952. (c) Aubin, S. M. J.; Sun, Z.; Pardi, L.; Krzystek, J.; Folting, K.; Brunel, L.-C.; Rheingold, A. L.; Christou, G.; Hendrickson, D. N. Reduced Anionic Mn₁₂ Molecules with Half-Integer Ground States as Single-Molecule Magnets. *Inorg. Chem.* **1999**, *38*, 5329–5340.